

# A Comprehensive Catalogue of Variable Stars in the field of 47 Tucanae.

David T F Weldrake

Research School of Astronomy and Astrophysics, Mount Stromlo Observatory, Cotter Road, Weston Creek, ACT 2611, Australia

[dtfw@mso.anu.edu.au](mailto:dtfw@mso.anu.edu.au)

Penny D Sackett

Research School of Astronomy and Astrophysics, Mount Stromlo Observatory, Cotter Road, Weston Creek, ACT 2611, Australia

[psackett@mso.anu.edu.au](mailto:psackett@mso.anu.edu.au)

Terry J Bridges

Anglo-Australian Observatory, P.O. Box 296, Epping. NSW, 1710, Australia  
Current Address: Department of Physics, Queen's University, Kingston, Ontario.  
K7L 3N6, Canada

[tjb@astro.queensu.ca](mailto:tjb@astro.queensu.ca)

and

Kenneth C Freeman

Research School of Astronomy and Astrophysics, Mount Stromlo Observatory, Cotter Road, Weston Creek, ACT 2611, Australia

[kcf@mso.anu.edu.au](mailto:kcf@mso.anu.edu.au)

Received \_\_\_\_\_; accepted \_\_\_\_\_

## ABSTRACT

We present the results of a comprehensive search for stellar variability in the globular cluster 47 Tucanae. Using the Mount Stromlo 40-inch (1m) telescope at Siding Spring Observatory and a combined V+R filter, we have detected 100 variable stars across a  $52\times 52'$  field centered on the cluster. The main aim of this project is to search for transiting 'Hot Jupiter' planets in this cluster, the results of which shall be discussed in a separate paper. Here we present the V+R lightcurves and preliminary investigations of the detected variable stars, which comprise 28 Eclipsing Binaries (21 contact binaries and 7 detached systems), 45 RR Lyrae stars (41 of which belong to the Small Magellanic Cloud and four seemingly to the Galactic Halo), and 20 K-giant Long Period Variables (LPVs). We also detected four  $\delta$  Scuti stars, one Type I Cepheid, and one Type II Cepheid. One variable appears to be a possible dust-enshrouded SMC star with a short period pulsation. Of these 100 variables, 69 are new discoveries. Our eclipsing binary sample indicates a clear radial segregation in period, and includes two binaries that are seemingly orbited by low-luminosity stellar companions. One RR Lyrae star shows a Blazhko effect with remarkable regularity.

Those variables previously known are cross-identified with Kaluzny and coworkers. In agreement with previous studies, this work shows that the relative frequency of detectable variable stars (particularly contact binaries) in 47 Tuc is very low compared to other studied regions. A distance modulus of  $18.93\pm 0.24$  for the Small Magellanic Cloud and  $13.14\pm 0.25$  for 47 Tucanae has been estimated from our sample, and are in agreement with values previously published.

The total database presented here contains V and I photometry for 43,067 47 Tuc field stars ( $13.0\leq V\leq 21.0$ ), along with 33-night V+R lightcurves and astrometry for 109,866 stars ( $14.5\leq V\leq 22.5$ ).

*Subject headings:* globular clusters: individual 47 Tuc (NGC 205) — binaries: general  
— stars: variables: other — blue stragglers — Cepheids — Delta Scuti — binaries:  
eclipsing — Galaxies: general (Small Magellanic Cloud)

## 1. Introduction

Variable stars in globular clusters (particularly binaries) play an important role in understanding cluster dynamical evolution. Despite this, such clusters have seldom been the targets of detailed study for the presence of variables, mainly due to the difficulty in obtaining accurate photometry from the ground of faint stars in very crowded fields. Due to technological advances in recent years, however, the number of clusters studied and the list of variable stars discovered has increased dramatically. As a general overview of the field, those major clusters investigated recently include Omega Centauri (Kaluzny et al. 1996, 1997; Haggard et al. 2003), M5 (Yan & Reid 1996), M71 (Yan & Mateo 1994), M4 (Kaluzny, Thompson, & Krzeminski 1997), NGC6397 (Kaluzny 1997), M22 (Pietrukowicz & Kaluzny 2003), NGC6946 (Guldenschuh, Layden, Welch, & Webb 2003), M69 (Gregorsok, Layden, Welch, & Webb 2003), M15 (Zheleznyak & Kravtsov 2003), M13 (Kopacki, Kołaczkowski, & Pigulski 2003) and M3 (Strader, Everitt, & Danford 2002). Yan & Cohen (1996) discovered six spectroscopic binaries in NGC5053. Clement et al. (2001) and Hut (1996) review recent and more historical studies into globular variables.

A few previous surveys have searched for variable stars in 47 Tuc. Sawyer Hogg (1973) discovered two variables. Edmonds et al. (1996); Edmonds & Gilliland (1996) used a HST dataset to detect 75 variable stars, including Eclipsing Binaries and variability among K-giants. Albrow et al. (2001) uncovered 107 variable stars, the largest number to date, and derived an overall binary frequency of  $14\% \pm 4\%$  using the same HST dataset as Gilliland et al. (2000) to search for Hot Jupiter planets in the cluster. Kaluzny et al. (1998) performed a wider field survey on the cluster, uncovering 42 variables.

We present a new extensive variable star catalogue, a natural byproduct of a photometric project to search for transiting 'Hot Jupiter' planets in 47 Tuc. The results of the planetary search will be the subject of a separate paper. The total catalogue comprises

28 Eclipsing Binary systems, 20 long period variables and 41 Small Magellanic Cloud (SMC) RR Lyraes, four Halo RR Lyraes, two Cepheids and four apparent  $\delta$  Scuti stars, and one anomalous short period Small Magellanic Cloud (SMC) star. Discrimination between cluster/SMC memberships is achieved using the location of the variable on the cluster Colour Magnitude Diagram. Our large number of new discoveries is due primarily to the very large field of view ( $52 \times 52'$ ) of our survey and also its photometric depth. In this paper, we present the phase-wrapped V+R lightcurves, preliminary investigations into the detected variable stars, and a description of our photometric, astrometric and lightcurve database.

Our survey covers a larger area than any previous search, and extends to deeper photometry than presented by Kaluzny et al. (1998). We recover 31 of Kaluzny's stars and discover a further 69 variables. The unrecovered variables either lie between CCDs, or within regions of no data caused by telescope offsets. The cluster core cannot be easily imaged by ground-based telescopes due to the extreme crowding. On our 300s exposures (V+R), the inner  $6'$  of 47 Tuc is saturated. The cluster field is located at a high galactic latitude ( $l=305.9$  deg,  $b=-44.9$  deg), providing low foreground contamination by the Milky Way and low reddening. The field is significantly contaminated by background stars from the Small Magellanic Cloud. Our field of view extends to  $\sim 60\%$  of the 47 Tuc tidal radius. Study of the SMC RR Lyrae stars, as standard candles, presents an opportunity to investigate the distance to the SMC from a location some seven degrees NW of the centre.

Contact eclipsing binaries (EcB) are very useful as distance indicators. Observing any double line spectroscopic binaries offers an opportunity to measure directly the primary stellar parameters such as mass, luminosity, radius and hence distance. Rucinski (1993) presents a method of distance determination for contact binaries by including the period, unreddened V-I colour and system metallicity. We present the results of an application of

Rucinski’s calibration for our binary sample with periods less than 1 day.

Section 2 describes the observations and data reduction, along with a description of the method used to obtain the lightcurves. Here we also discuss the astrometry and variable detection methodology, along with notes on cluster membership of the variables. Our survey completeness and the quality of the photometry is described. Section 3 deals with the cluster Colour Magnitude Diagram (CMD), the corresponding photometric database, and describes the photometric calibrations. Section 4 contains a discussion and preliminary analysis of the different types of variables in the catalogue and presents their lightcurves. We summarise and present conclusions in Section 5. Finder charts of these stars are provided on a webpage link to allow easy identification on 47 Tuc wide field images.

## 2. Observations and Data Reduction

This project was undertaken using the Australian National University (ANU) 40-inch (1m) telescope at Siding Spring Observatory. We used the Wide Field Imager (WFI) which consists of a  $4 \times 2$  array of  $2048 \times 4096$  pixel back-illuminated CCDs. The CCDs are arranged to give a total format of  $8K \times 8K$  pixels. The detector scale is  $0.38''/\text{pix}$  at the 1m telescope Cassegrain focus, with a field of view of 52 arcmin on a side. This very large field allows us to image much of 47 Tuc, approaching 60% of the cluster tidal radius of 45.9 arcminutes (Leon, Meylan, & Combes 2000) in one exposure. The field layout is presented in Fig.1. Our main aim of detecting planetary transits requires an effective SN ratio of 200 or more at  $V=18$  for a  $3\sigma$  detection and, to maximise the in-transit sampling, exposures no longer than 300s were employed. Our broadband filter covers the combined wavelength range of Cousins V and R, giving a significant increase in signal-to-noise while maintaining the image degradation due to atmospheric dispersion at an undetectable level. From previous experience with this filter, for a star of  $V=18.5$  in  $2''$  seeing, the photon noise S/N decreases

from 220 at 7-day moon to 165 at bright moon.

The globular cluster 47 Tucanae was observed for a total of 33 nights from 2002 August 22 to 2002 September 24 with a field centre of RA=00h24m05.2s DEC= $-72^{\circ}04'51.0''$ . Approximately 80% of the observing time was useful for the main planetary transit project, with mean seeing of 2.2 arcsec. The temporal coverage of the cluster was maximised as much as possible; and averaged an image every 6 minutes for around 10 hours per night. Each image was checked for quality independently after readout. Unsuitable images caused by satellite trails, bad seeing periods, etc, were discarded.

In total we have 1220 images of the same field centered on 47 Tuc, which have been used to produce time-series lightcurves for 109,866 unsaturated stars, with apparent magnitude  $14.5 \leq V \leq 22.5$ . This covers a large range of stellar mass and type, encompassing most of the red giant branch (RGB) the subgiant branch, the cluster turn-off, and the cluster main sequence down to a magnitude of  $V=22.5$ . This dataset therefore covers a large range of variable types.

Initial reduction of the raw images was undertaken using the MSCRED package of IRAF <sup>1</sup>. A significant number of calibration images were obtained over the 33-night run, and allowed for correction of time-dependent variations, eg., differences in flat fields from one observing period to the next, across the WFI array. Initial reductions included region trimming and overscan correction, bias correction, flat-fielding and dark current subtraction. A dark-sky flat was obtained, but was not used because it degraded the large scale image quality. After checking the final reduced images for flatness (using IMSTAT)

---

<sup>1</sup>IRAF is distributed by National Optical Observatories, which is operated by the Association of Universities for Research in Astronomy, Inc., under cooperative agreement with the National Science Foundation

and pixel-to-pixel variations, the resultant 1220 object images were then ready for the main photometric pipeline and analysis.

## 2.1. Photometry

The primary photometric method to generate lightcurves was carried out using a Difference Image Analysis (DIA) method originally described as a optimal PSF matching algorithm by Alard & Lupton (1998), and modified by Wozniak (2000). Detailed discussion of each program making up the pipeline can be found in Wozniak’s paper. We summarize the method here. DIA consists of the following steps: Firstly, all frames are transformed onto a common coordinate system. Then a template image is produced by combining the best quality images with small offsets into a master image. The Point Spread Function (PSF) of the stars on each image is determined using a combination of two Gaussians, one for the core and one a factor of 1.83 wider for the wings, each multiplied by a third order polynomial. The best PSF-matching kernel is found and each image is then subtracted from the template (reference) frame. The coordinates of all stars on the template images are found, and finally the profile photometry is extracted from those star positions.

Central to this method is the assumption that the pixels containing PSF information in the analysis image vary only slightly due to seeing variations. *A priori* knowledge of the PSF and the sky background is not required, and the method works better as the crowding increases, as in denser fields a larger number of pixels contain information about any PSF differences. Heavy blending can cause trouble, however, as the pipeline photometry does not model surrounding stars and thus faint and/or heavily blended objects can be contaminated by neighbouring stars. For this reason, a crowding flag is introduced: a flag of 1 indicates that a pixel brighter than  $0.15 \times \text{distance in pixels} \times \text{pixel flux}$  lies within the immediate four pixel neighbourhood. For the production of the PSF, a star is rejected



if another local maximum at least  $2\sigma$  above the background level is present.

For ease of data handling, each of the eight WFI CCDs were cut into 32 subsections of  $512 \times 512$  pixels each. Once the images were reduced, the 45 exposures with the best mean seeing, measured at  $1.1''$  were then coadded to create a template frame, a very high signal-to-noise version of each subsection. This allowed initial flux measurements of the stars to be made, which defines the zero point of the output lightcurves. The coordinates of all the stars detected by DAOFIND on these  $512 \times 512$  template images were fed into the main photometric pipeline. Those stars within 22 pixels of the subframe edge were discarded; due to telescope pointing offsets those stars do not have complete temporal coverage. Due to these offsets,  $\sim 21,000$  stars ( $\sim 15\%$  of total) could not be produced for the final lightcurve database.

After the subtraction process is complete, the derived centroid of any variable object is unbiased by surrounding unvarying stars. The DIA method measures the flux differences between the frames, rather than the total flux. The lightcurve of the variable object can be converted to total flux units using the stellar flux from the template.

As originally implemented, the method automatically detects objects that are classified as variable from frame to frame using the following conditions: At least three consecutive points depart by at least  $3\sigma$  from the baseline in the same sense, and there are at least 10 points departing by  $4\sigma$  from the baseline in either sense. The method then produces a lightcurve at the pixel coordinates of the detected varying object. As the main aim of the project was to find the periodic  $\sim 1\text{-}2\%$  drop in brightness caused by a planetary transit, which is practically undetectable by this automatic process, we altered the method slightly. The program was forced to produce a lightcurve for every visible star on our best-seeing image, which yielded the largest number of stars of any of our dataset images. Using DAOFIND within IRAF, the pixel locations of all stars were determined. The main

photometric pipeline within DIA was then instructed to produce a lightcurve for each of these locations. The variable stars presented in this paper were detected using this modified method. This implementation of the method gave us a total 1200-point lightcurve database across the 47 Tuc field for 109,866 unsaturated stars. This is a smaller number than that of our total astrometric database, due to telescope offsets and the gaps between images.

The DIA method produces lightcurves that are not on a standard magnitude system. The lightcurves are produced with linear flux units, from which a constant reference flux taken from the template images has been subtracted. To convert this unit into a magnitude scale, the flux of each star on the reference image must be determined. An estimate of the flux was made by running DAOPHOT on the reference template images and measuring the flux (in counts) for each star. The change in light output in magnitudes can then be calculated via:

$$\Delta m_i = -2.5 \log[(N_i + N_{\text{ref},i})/N_{\text{ref},i}]$$

where  $N_{\text{ref},i}$  is the flux of star  $i$  on the template image, and  $N_i$  is the difference flux on a given frame in the time series. We then compared our range of  $\Delta m_i$  for those variables found by Kaluzny et al. (1998) for verification. These  $\Delta m_i$  are thus used as the magnitude total variability level of our detected variables. Fig.2 shows the amplitude comparison between the two datasets for those variables which can be crossidentified, and shows a scatter around the zero-point with a mean of -0.0016 and a standard deviation of 0.13 magnitudes. The slope of the LPV variables towards fainter magnitudes is attributed to the different passbands of Kaluzny et al. (1998) (V) and ourselves (V+R). Those EcB which are not close to the zeropoint are members of the binary main sequence, and hence are more likely to be composed of different colour components. The RR Lyrae scatter is attributed to the relative faintness of this sample.

Our photometric errors are presented in Fig.3, which shows the V+R rms photometric uncertainties of our lightcurves as a function of V magnitude. As we have a significant change in crowding between the inner four CCDs and the outer four (see Fig.1), two rms curves are presented. It can be seen that the outer CCDs produce comparable lightcurve quality for stars up to 0.5mag fainter for any given rms level compared to the inner CCDs. We therefore have sufficient photometric precision to detect a 1.5-2.5% dip (typical of the general range of a 'Hot Jupiter' planet (Charbonneau, Brown, Latham, & Mayor 2000) in the lightcurves of V=18.5 stars in a crowded inner CCD and V=19.0 in an uncrowded outer CCD. This limit allows us to probe the brightest 1.5-2 magnitudes of the cluster main sequence for any orbiting giant planets; these results will be presented in a subsequent paper. Our rms precision also allows us to detect variable stars to V~21 with amplitudes of (0.14,0.20) magnitudes for the two crowding levels, giving us an excellent chance to detect previously unknown variable stars. Fig.4 shows the magnitude depth of our photometry for all eight CCDs, with recovered stars counted in 0.25 magnitude bins. Our photometry is limited to the range  $13.0 \leq V \leq 22.0$ , with different chips having slightly different sensitivities. The apparent peaks in the stellar distributions are due to incomplete sampling at faint magnitudes. The gradual decrease in star numbers towards CCD8 can be clearly seen, indicative of increasing distance from the Small Magellanic Cloud (SMC), and hence decreasing background contamination.

## 2.2. Astrometry

Astrometry was obtained for all 143,814 stars detected in our best seeing image, across the eight CCDs of the 47 Tuc field allowing a determination of the position of all stars in both our photometric and lightcurve database. We used a program to search the USNO CCD Astrograph Catalogue (UCAC1) for astrometric standard stars within

the field (B.P.Schmidt, 2003 private communication). Several hundred such stars were cross-identified, allowing for an accurate determination of the astrometric solution of our star lists. The rms residual of the astrometry was  $\sim 0.15$  arcsecs. Our astrometry is presented in Fig.1, with the CCD number overplotted. The cluster core and our extensive coverage of the cluster is apparent.

### 3. Colour Magnitude Diagram

The V,V-I Colour Magnitude Diagram (CMD) used in the production of the variable colour data is presented in Fig.5. These data were originally taken at the MSSSO 40" telescope by Ken Freeman and Michelle Doherty to allow for a placement of any candidate transiting system on the V,V-I system. The data cover the same  $52 \times 52'$  FOV as the lightcurve dataset presented in this paper, and totalling 43,067 stars. The magnitude range is  $13.0 \leq V \leq 21.0$  in V and I. The CMD was calibrated against that presented by Kaluzny et al. (1998). The authors warn in that paper of systematic errors caused by non-linearity of the OGLE CCD chip. For faint stars these errors are likely to be more significant. The OGLE dataset as available on their website (calibrated) was overplotted on top of our uncalibrated CMD data. Our data was then shifted until the two datasets overlay each other. A histogram of the distribution of the stellar magnitudes was produced, and our data was shifted further until a more accurate match was found by comparing the V magnitude of the Horizontal Branch. This was repeated for V-I calibration. This simple calibration method produced photometry accurate to  $\leq 0.03$  mag, across the full magnitude range. Fig.5 shows our CMD. Variable stars in the V+R dataset were cross-identified by comparing the template image containing the variable and the corresponding CCD image of the CMD dataset. The V and V-I information in Tables 3,4 and 5 are associated with uncertainties of 0.03 and 0.04 respectively, and are the non-random errors in the zero-point

determination and incorporate the errors in the OGLE calibration.

### 3.1. Method for variable detection.

A Lomb-Scargle Periodogram (LSP) method was chosen to search for periodic variables in the final lightcurve database (Bretthorst 2001). This method was produced specifically to overcome the problem of unevenly spaced data, which in our case is caused by daylight and cloudy nights. A Fourier power spectrum is produced, with the same statistical properties as a standard power spectrum. If a periodicity (P) is detected in the data, a spike is produced in the spectrum at a frequency of  $2\pi/P$ . As implemented, any spike above  $2\times$ rms of the power spectrum is identified as a candidate. Using this condition, 29,314 lightcurves which contained such an apparent periodicity ( $\sim 23\%$  total database,  $\sim 300$  times the final variable number) were found, which were then examined in detail. It was noticed that the vast majority of this list was composed of common systematic effects inherent in the data, lightcurves from stars close to saturation, stars very close to our magnitude limits and the  $>2\sigma$  variables. All those candidates which exhibited a clear periodicity by eye were catalogued, leaving a sample of 100 for the variable list. Fig.6 shows our detection limits. The log of the total amplitude (in magnitudes) of the detected variables have been plotted against V. It is clear that there is a sharp cutoff to the detections, marked with a dotted line. Any amplitudes which are  $>3\%$  are detectable to  $V=17.0$ , and only those with an amplitude  $>1$  mag can be found for  $V>22$ . Hence those variables which lie underneath this limit are missed in our dataset.

By phase-wrapping the candidate lightcurves at the detected period, the nature of the periodicity is seen. The LSP-derived period is very close  $\sim 0.03d$  to the chosen 'true' periods presented for our variables in Table1. Once phase-wrapped, the period was altered (at the third significant figure) until a minimum in the scatter of the points was seen; this value

was recorded as the period of the variable. Our cross-identified variables had their derived periods compared to those in (Kaluzny et al. 1998), and are in excellent agreement.

## 4. Preliminary Variable Analysis

### 4.1. Eclipsing Binaries

Phase-wrapped lightcurves of all 100 variable stars detected in our dataset are presented in Figs.7-16. We arrange the lightcurves by type, EcB (Figs.7-9), RR Lyraes (Figs.10-13), long period variables (LPVs, Figs.14-15) and miscellaneous variables (Fig.16). For the EcB, it is clear that examples of contact (ie V6), semi-contact (ie V7) and detached configuration (ie V69) binaries are present, classified due to the appearance (or lack thereof) of features in the lightcurves indicating tidal distortion of the stellar components, the period, and the length of time between eclipses. The EcB sample consists mostly of W Ursae Majoris-type lightcurves, with short periods. Most of these stars seem to be candidate blue stragglers with cluster membership (see Fig.17). The lightcurves of some of these stars (ie, V6, V7, V12) display secondary variations outside the main variability, which could be indicative of star-spots, flares or Roche-Lobe overflow between the components (E.C Sung, 2003 private communication). One of the main explanations for the phenomenon of Blue Straggler Stars (BSS) is that the two binary components are transferring mass, and hence remain on the main sequence when they otherwise would have evolved off. Leonard (1996) showed that many BSS are members of short-period binaries, and as such are likely to be transferring material from one to the other as one component evolves. Hence it is not surprising that some of our sample of Blue Stragglers (ie V6) seem to show evidence of such mass transfer activity in their lightcurves.

A number of EcB appear to lie on the cluster Binary Main Sequence (BMS) and as

such all are very likely members of 47 Tuc. Detached systems are also seen in the sample (V39, V41, V69, V78, V84, V89 and V93). Of these, four do not show detectable secondary eclipses to our rms level (V69, V78, V89, V93), and thus could conceivably be orbited by low luminosity companions, most likely M-dwarfs. Our data for V78 and V93 is very limited, with only one eclipse visible across our temporal range. Our period estimates for these two variables are therefore not well determined. We have estimated a period for these two stars which would hold if all other eclipses occurred during cloud or daylight. Further observations are required to derive an accurate period. If these stars are indeed orbited by M-Dwarfs, these variables would be important to determine the survivability and long-term stability of such low-mass companions inside globular clusters (Adams & Laughlin 2003). We present phase wrapped lightcurves of these two 'special cases' in Fig.18, with the eclipses plotted more clearly than in the general lightcurve database figures. V78 also shows an apparent variation at 1.015d, as well as the longer period for which only one eclipse is seen. This is shown in Fig.8 (two plots for V78), and as the period is so close to 1 day, it is almost certainly due to terrestrial effects. It is included for completeness. The lightcurve data suggest that the companion sizes are approximately 0.25-0.3 Solar radius, assuming a mid-to late K-type primary at the distance of 47 Tuc. The rest of our EcB sample are detached binaries on the cluster BMS.

The apparent frequency of the occurrence of detectable 47 Tuc contact binaries in the field is  $21/124073 \approx 1.7 \pm 0.4 \times 10^{-4}$ , which is slightly higher, but consistent with, the estimate of  $1 \times 10^{-4}$  presented in Kaluzny et al. (1998), and is more than an order of magnitude lower than that observed in the core of 47Tuc (Albrow et al. 2001), and in fields containing Galactic open clusters (Kaluzny & Rucinski 1993) and OGLE fields located in Baade's Window, close to the Galactic Centre (Rucinski 1997). The reasons for this difference are unclear, although mass segregation may play an important role in determining the radial distribution of such stars. For comparison, some other globular clusters studied

with variability surveys give eclipsing binary frequencies of  $7.5 \times 10^{-4}$  for M71 (Yan & Mateo 1994) and  $1.4 \times 10^{-3}$  for M5 (Yan & Reid 1996).

Our dataset shows an apparent segregation in binary period, with shorter period binaries located closer (in projection) to the core of 47 Tuc. This can be seen clearly in Fig.19 where we have plotted the number of contact and detached EcB as a function of radius from the core in bins of 6 arcminutes. A (normalised) histogram of the total star population has been overplotted for comparison. The two EcB distributions are clearly different, with a significance of around  $4\sigma$ , as determined by a Kolmogorov Smirnov test. Contact systems are preferentially located closer to the core (in projection) than detached systems of the same magnitude. This segregation is not a classical indication of mass segregation, for which we would expect both detached and contact binary systems to be preferentially located closer to the core, but may be an indication of dynamical effects, with binaries closer to the core having lost much of their orbital energy. The binaries further out retain their energy, and hence remain in longer period orbits. Due to dynamical effects, it is expected that most of the cluster contact binaries would be located in the core (Hut et al. 1992), although some would have been ejected from the core by star-star encounters. A theoretical King Profile has also been overplotted to show the total stellar distribution, without the crowding our data suffers towards the core. The inner  $6'$  is not sampled in our dataset; the dropoff on binary number at the inner 6 arcminutes is entirely due to this effect.

Fig.20 shows the sample of our contact EcB (periods  $\leq 0.5$ d) indicating a clear relationship between Period and V-I colour. This period-colour relationship was first noted by Eggen (1967), and further investigated by Rubenstein (2001). The explanation as offered by these authors is that this relation is indicative of the differing system masses, the higher mass systems are bluer and have longer orbital periods than the lower mass systems. As



one moves further down the cluster CMD (in our case), the mass of the system in total decreases, and the overall system colour gets redder. Since massive stars are physically larger than low-mass stars, those binaries which have high mass components must have a greater orbital separation to accommodate this larger stellar volume. Therefore the lower the likely masses of the components the redder they appear, and the shorter the orbital period will be. System metallicity has a bearing on the positions of the contact binaries in the period colour relationship. Yan & Mateo (1994) showed that the reduced line blanketing of metal-poor stellar atmospheres accounted for some of the differences between a globular cluster period colour relationship and that of field binaries. The lower metallicity also makes stellar radii smaller, affecting the resultant orbital period for such systems.

#### 4.2. Notes on cluster membership

We do not have definitive proof that our variable stars are members of 47 Tuc, the background SMC, or the Galactic halo. Spectroscopic observations are required to confirm membership; the heliocentric radial velocity of 47 Tuc (-19.4km/s; Richter, Tammann, & Huchtmeier 1987) is very different to that of the Galactic halo and the SMC (+158km/s; Mayor et al. 1984). In this paper, we have estimated membership for variables from their location on the cluster Colour Magnitude Diagram (CMD), which is shown schematically in Fig.17. As a globular cluster, 47 Tucanae has a very small spread of stellar metallicity, so that the stars lie on tight loci on the cluster CMD, without the spread in colour observed in other objects such as the SMC. As such, we can preliminarily assign memberships which are presented in Tables 1-5. For the contact eclipsing binary (EcB) systems, we have adopted Rucinski’s absolute brightness calibration (Rucinski 1993) to calculate  $M_V$ , distances and thus memberships. The method estimates  $M_V$  from the period, unreddened colour, and system metallicity via:

$$M_V^{cal} = -4.43 \log(P) + 3.63(V - I)_O - 0.31 - 0.12 \times [\text{Fe}/\text{H}].$$

For all our EcB systems, we have adopted  $[\text{Fe}/\text{H}]=-0.76$  and  $E(V-I)=0.05$  (Harris 1996). Fig.21 shows the derived distance modulus of all EcB for which we have complete colour information and have periods  $P < 1\text{d}$ ; such systems can be regarded as contact systems. The derived distance modulus (DM) of 47 Tuc from this plot is  $13.14 \pm 0.25$ , which is in agreement with the estimate of 13.21 presented by Harris (1996), and that derived by Percival, Salaris, van Wyk, & Kilkenny (2002), using main sequence fitting, of  $(m - M)_V = 13.37_{-0.11}^{+0.10}$ . From Fig.21, it is clear that we have detected 10 eclipsing binaries that are likely members of 47 Tuc. V95 and V26 appear to be foreground members of the Galactic halo, whereas V20 is a likely member of the Small Magellanic Cloud (Harries, Hilditch, & Howarth 2003). Interestingly, V11 and V75 both have distance moduli which lie inbetween 47 Tuc and the SMC. It is interesting to note the very small amplitude of variation associated with the foreground EcB V26, perhaps indicating low mass components.

To estimate the total number of variable stars present in the WFI field we consider how many of (Kaluzny et al. 1998)'s sample we missed due to telescope offsets and gaps between our CCDs. We recovered 31 of the 42 variables presented in that paper. Using this result, we estimate that we missed  $\sim 26\%$  of the variables we are capable of detecting. We therefore expect that in total there are  $126 \pm 11$  detectable variable stars present in the field.

### 4.3. RR Lyraes

A significant number of Small Magellanic Cloud (SMC) RR Lyrae stars were found in our data. Their phase-wrapped lightcurves are presented in Figs.10-13, along with a preliminary examination. All but four RR Lyrae stars are clustered around  $V=19.68$ , indicating their membership in the SMC. The other four stars are very likely to be located

in the Galactic halo, one of which (OGLEGC223=V10) was presented in Kaluzny et al. (1998). Three populations of RR Lyrae stars are found in our data: type AB, type C, and two examples of RR Lyrae stars with periods of about 1 day. These latter stars (type AHB1) are described by Sandage, Diethelm, & Tammann (1994), and constitute very low metallicity post-horizontal branch (HB) stars passing rapidly through the instability strip in the vicinity of the Horizontal Branch but on bright evolutionary tracks (Strom, Strom, Rood, & Iben 1970). Both of our AHB1 stars are Galactic Halo stars, and hence indeed likely to be of a low metallicity. The identification of these AHB1 stars is presented in the RR Lyrae period distribution (Fig.22), and are also identified on the RR Lyrae P-V diagram (Fig.23).

By comparing the density of RR Lyraes in our sample with those previously published for the field of 47 Tuc, we can draw conclusions about the completeness of our RR Lyrae sample. Graham (1975) searched for variables in an area covering 4680 arcmins<sup>2</sup> north of 47 Tuc, which included a small part of the cluster. The RR Lyrae density presented in that paper was 0.016 variables per square arcminute, and is the generally accepted value for the RR Lyrae density in this region of the sky. The surface area covered by our search is 2704 arcmin<sup>2</sup>, and yields a derived RR Lyrae density value  $\approx 0.016 \pm 0.003$  RRLyr/arcmin<sup>2</sup>, consistent with the Graham (1975) result. The limiting magnitude of Graham’s search was  $B \approx 20.3$ , whereas ours is  $V+R \approx 21.0$ . We did not identify any 47 Tuc RR Lyraes in our dataset, due to their relative brightness compared to our target stars. With our 300s exposures, at  $V=14.06$  (Leon, Meylan, & Combes 2000) such cluster stars would be very close to saturation.

Fig.23 shows the period-luminosity diagram for our sample of RR Lyraes. Those that lie in the SMC are easily distinguishable from those that lie in the Galactic Halo (marked with a H). The long-period AHB1 RR Lyraes are also identified. The average V magnitude

of the SMC stars lies at  $V=19.68\pm 0.24$ . The mean  $V$  absolute magnitude of RR Lyraes in the SMC is  $M_V(\text{RR})=0.75$ , as assumed by Graham (1975), and also used by Kaluzny et al. (1998) and includes correction for metallicity effects. It therefore follows that the SMC distance modulus  $(m-M)_V$  from our sample of RR Lyraes is  $18.93\pm 0.24$  or  $61.45\pm 7.0$  Kpc. The large errorbar is due to the relatively small sample size. The average magnitude of each of the RR Lyrae stars was found, by integrating across the lightcurve, and then the phase of the variability amplitude at the time of the CMD dataset was used to determine the actual apparent magnitude at this same time. The difference between this and the mean magnitude was then measured. The error in this measurement as plotted on Fig.23 was taken as the residual scatter in the phase-wrapped lightcurve points at this time. This method allows us to account for the variability amplitude when finding the  $V$  magnitudes of our stars, and hence a more accurate measure of the SMC distance. Our result compares favourably with that of  $18.89\pm 0.10$  presented by Harries, Hilditch, & Howarth (2003). A larger sample size would help to indicate more conclusively if the SMC is extended in the radial dimension towards the direction of 47 Tuc.

The Blazhko Effect is a little understood feature of some RR Lyrae stars, in which the amplitude of variation itself varies with a certain periodicity. One popular theory to explain this erratic behaviour is that it is related to the presence of a strong photospheric magnetic field (Cousens 1983), yet recently Chadid, Wade, Shorlin, & Landstreet (2004) has ruled out a magnetic field for the brightest Blazhko (BL) star - RR Lyrae itself, the prototype of the class. Neither this, nor the rotating resonant pulsator model (Dziembowski & Cassisi 1999) explain observed BL star properties. The frequency of such BL stars seems to be dependent on the metallicity of the environment in which they occur, Alcock et al. (2003) has found a different incident rate of BL stars in the LMC ( $\sim 11\%$ ) when compared to Moskalik & Poretti (2003), who found a 23% incidence rate for the Galactic Bulge. Both papers agree that metallicity is the most probable reason. The reason for BL behaviour in

general therefore remains unknown. It is seen on a few of our RR Lyrae sample (V2, V3, V18, V86). Fig.24 shows the remarkable regularity of the Blahzko Effect for V86, for which we plot the phase-wrapped lightcurve over four periods. The amplitude of the variation decreases significantly over three primary periods. This behaviour was constant over the whole 33-night run. The other three Blahzko examples do not show such regularity. A few of the RR Lyrae lightcurves show significant scatter, primarily due to crowding, and variable seeing.

#### 4.4. Long Period Variables

Our sample of variables also includes 20 Long Period Variables (LPVs) with locations on the CMD that are consistent with two main populations: those present in the red giant branch (RGB) of 47 Tuc itself, and those which lie on the AGB/RGB of the SMC. We define a long period as being significantly longer than that of RR Lyrae and EcB stars, from about 5-6 days. Stars with very long periods cannot have their periods accurately determined from our dataset, as our temporal coverage is insufficient to show even a single period; we present lower limits on the periods of the more extreme LPVs. Some of these stars were found by Kaluzny et al. (1998). These extreme LPVs are likely to be examples of AGB stars (Miras) in the SMC. V27 (OGLEGC230) is affected by bad seeing and extreme crowding, and hence has significantly more scatter on its lightcurve. Our derived period for this star is half that derived by Kaluzny et al. (1998), who indicated that their period might require revision.

Only about six of our LPV sample can be given tentative 47 Tuc membership, a number too small to give meaningful results to study their radial distributions. It is very likely that the majority of cluster RGB variables are brighter than our magnitude limit. A shorter exposure search for variability among 47 Tuc RGB stars has recently been started

by Kiss et al (2003, private communication, also with WFI on the MSSSO 40-inch), and our LPV sample will overlap somewhat with their results. This should allow a more accurate study into the cluster LPV radial distribution.

#### 4.5. Other Variables

A small number of other variables were also discovered in our dataset, including two Cepheids, four  $\delta$  Scuti stars, and an anomalous short-period red variable, which is a likely SMC star. The two Cepheids (V24 and V37) are identified from their position in the schematic cluster CMD (Fig.17). They are significantly brighter and redder than the RR Lyrae stars, but are of short period (0.387d and 2.572d respectively) for Cepheids, and as such could be classified as anomalous. V24 has been tentatively identified as a TypeII Cepheid based on the secondary variation seen on the lightcurve at phase  $\sim 0.5$ .

We detected four  $\delta$  Scuti stars in our search (V35, V54, V67 and V80). All are certainly members of the SMC, as they have  $V \sim 21$ . This is at the limit of our detectability, but they were found due to their large amplitude of variation. V35, V54 and V67 all have very short periods  $< 0.1$ d, typical of  $\delta$  Scuti stars. V80 has a period that is longer, at 0.2144d, and is among the faintest variables in our catalogue at  $V \sim 22$ . It has been classified as a  $\delta$  Scuti star due to the shape of the lightcurve, and the amplitude of variation. The  $\delta$  Scuti lightcurves presented here show a significant amount of scatter, which is attributed to photometric scatter caused by the faintness of the sample. To investigate the possibility of multi-periodicity, the periodograms for these four stars were compared to those of non-variables of the same magnitude. The lightcurves were phase-wrapped to all significant periods found with the LSP (see earlier), the majority of the extra periodicities were found to be common, and attributed to systematic effects. No obvious secondary period was seen for these stars down to our sensitivity level. The amount of photometric scatter at  $V \sim 21$  is

$\sim 0.3$  mag, and is consistent with the scatter seen on these four lightcurves.

Finally, from its position on the schematic CMD V60 is an apparent SMC AGB star, with  $V-I=2.99$ , yet a periodicity of only 0.2544d. The amplitude of variation is moderate ( $\Delta\text{mag}\sim 0.1$ ), and as such indicates an apparent giant red star with a very short period pulsation. It follows that such a star would likely be unstable at such short periods. At the distance of the SMC derived above, the absolute magnitude would be  $-1.8$ , typical of an A-type star. It therefore seems likely that this star is actually much bluer, but could possibly be a post-AGB star surrounded by a dusty shell. Future monitoring and imaging of this star would be useful to unravel the mystery.

## 5. Summary and Conclusions

We have presented data for 100 variable stars detected across a wide ( $52\times 52'$ ) field centered on the globular cluster 47 Tucanae. Of these 100, 69 are new discoveries. The sample consists of 41 apparent Small Magellanic Cloud RR Lyrae stars, four Halo RR Lyrae stars, 28 eclipsing binaries, 20 Long Period Variables, four  $\delta$  Scuti Stars and two Cepheids. We also detected one anomalous short period red giant, perhaps surrounded by a dusty region. Four of our RR Lyrae sample display Blazhko Effect variations, one with remarkable regularity. This catalogue more than doubles the number of known variables in the 47 Tuc field. Of the EcB sample, four variables are perhaps orbited by faint companions, most likely M-Dwarf stars. Such stars are important in determining the long-term stability and survivability of low-mass objects in close orbits inside globular clusters. Future spectroscopic observations of these candidates are planned. As well as presenting this new variable catalogue, this paper presents a new complete database of V and I photometry, astrometry and 33-night V+R lightcurves for 109,866 stars across the field. The distance modulus of both 47 Tucanae and the SMC have been determined from

our sample. The values are consistent with those already published for these two objects.

It is clear from the eclipsing binary results, as well as those previously published in the literature, that the relative frequency of contact binaries in the field of 47 Tuc is very low compared to other studied regions. The reasons for this difference are unclear, although mass-segregation and dynamical effects seem to play an important role. Our sample of EcB shows a distinct period/radial-distance segregation, perhaps indicative of dynamical relaxation. Quite possibly the more massive shorter period contact binaries are located preferentially within the cluster core, an unsampled area in our experiment.

### **Acknowledgments**

The authors wish to thank the following people for their help in the producing this piece of work: Matthew Coleman for helping the first author relieve the insanity of observing for 33 nights straight; Eduard Westra for help in debugging the photometric pipeline, and for answering many emails to that effect; Brian Schmidt for allowing use of his astrometric package, as well as instructions on its operation; Laszlo Kiss for looking over some of the lightcurves and clearing up the identifications of the more noisy variables, and Doug Welch for helpful comments while acting as referee.

Finding charts for all variables are available on the Electronic edition of this paper. The orientation of these charts has north to the top and east to the left, produced from the corresponding template image which contains the variable, and they are each  $3.24'$  on a side.



## REFERENCES

- Adams, F. C. & Laughlin, G. 2003, *Icarus*, 163, 290
- Alard, C. & Lupton, R. H. 1998, *ApJ*, 503, 325
- Albrow, M. D., Gilliland, R. L., Brown, T. M., Edmonds, P. D., Guhathakurta, P., & Sarajedini, A. 2001, *ApJ*, 559, 1060
- Alcock, C., et al. 2003, *ApJ*, 598, 597
- Bretthorst, G. L. 2001, *AIP Conf. Proc.* 568: Bayesian Inference and Maximum Entropy Methods in Science and Engineering, 568, 241
- Chadid, M., Wade, G. A., Shorlin, S. L. S., & Landstreet, J. D. 2004, *A&A*, 413, 1087
- Charbonneau, D., Brown, T. M., Latham, D. W., & Mayor, M. 2000, *ApJ*, 529, L45
- Clement, C. M. et al. 2001, *AJ*, 122, 2587
- Cousens, A. 1983, *MNRAS*, 203, 1171
- Dziembowski, W. A. & Cassisi, S. 1999, *Acta Astronomica*, 49, 371
- Edmonds, P. D., Gilliland, R. L., Guhathakurta, P., Petro, L. D., Saha, A., & Shara, M. M. 1996, *ApJ*, 468, 241
- Edmonds, P. D. & Gilliland, R. L. 1996, *ApJ*, 464, L157
- Eggen, O. J. 1967, *MmRAS*, 70, 111
- Gilliland, R. L. et al. 2000, *ApJ*, 545, L47
- Graham, J. A. 1975, *PASP*, 87, 641

- Gregorsok, J. D., Layden, A. C., Welch, D. L., & Webb, T. M. A. 2003, American Astronomical Society Meeting, 203,
- Guldenschuh, K. A., Layden, A. C., Welch, D. L., & Webb, T. M. A. 2003, American Astronomical Society Meeting, 203,
- Haggard, D., Dorfman, J. L., Cool, A. M., Anderson, J., Baily, C. D., Edmonds, P. D., & Grindlay, J. E. 2003, American Astronomical Society Meeting, 203,
- Harries, T. J., Hilditch, R. W., & Howarth, I. D. 2003, MNRAS, 339, 157
- Harris, W. E. 1996, AJ, 112, 1487
- Sawyer Hogg, H. 1973, JRASC, 67, 8
- Hut, P. et al. 1992, PASP, 104, 981
- Hut, P. 1996, IAU Symp. 174: Dynamical Evolution of Star Clusters: Confrontation of Theory and Observations, 174, 121
- Kaluzny, J., Kubiak, M., Szymanski, M., Udalski, A., Krzeminski, W., & Mateo, M. 1996, A&AS, 120, 139
- Kaluzny, J. 1997, A&AS, 122, 1
- Kaluzny, J. & Rucinski, S. M. 1993, ASP Conf. Ser. 53: Blue Stragglers, 164
- Kaluzny, J., Kubiak, M., Szymanski, M., Udalski, A., Krzeminski, W., & Mateo, M. 1997, A&AS, 125, 343
- Kaluzny, J., Thompson, I. B., & Krzeminski, W. 1997, AJ, 113, 2219
- Kaluzny, J., Kubiak, M., Szymanski, M., Udalski, A., Krzeminski, W., Mateo, M., & Stanek, K. Z. 1998, A&AS, 128, 19

- Kopacki, G., Kołaczkowski, Z., & Pigulski, A. 2003, *A&A*, 398, 541
- Leon, S., Meylan, G., & Combes, F. 2000, *A&A*, 359, 907
- Leonard, P. J. T. 1996, *ApJ*, 470, 521
- Mayor, M. et al. 1984, *A&A*, 134, 118
- Moskalik, P. & Poretti, E. 2003, *A&A*, 398, 213
- Percival, S. M., Salaris, M., van Wyk, F., & Kilkenney, D. 2002, *ApJ*, 573, 174
- Pietrukowicz, P. & Kaluzny, J. 2003, *Acta Astronomica*, 53, 371
- Richter, O.-G., Tammann, G. A., & Huchtmeier, W. K. 1987, *A&A*, 171, 33
- Rubenstein, E. P. 2001, *AJ*, 121, 3219
- Rucinski, S. M. 1993, *PASP*, 105, 1433
- Rucinski, S. M. 1997, *AJ*, 113, 1112
- Sandage, A., Diethelm, R., & Tammann, G. A. 1994, *A&A*, 283, 111
- Strader, J., Everitt, H. O., & Danford, S. 2002, *MNRAS*, 335, 621
- Strom, K. M., Strom, S. E., Rood, R. T., & Iben, I. J. 1970, *BAAS*, 2, 347
- Yan, L. & Reid, I. N. 1996, *MNRAS*, 279, 751
- Yan, L. & Mateo, M. 1994, *AJ*, 108, 1810
- Yan, L. & Cohen, J. G. 1996, *AJ*, 112, 1489
- Westra, E.A.M. 2003, Masters thesis at Rijksuniversiteit Groningen
- Wozniak, P. R. 2000, *Acta Astronomica*, 50, 421

Zheleznyak, A. P. & Kravtsov, V. V. 2003, *Astronomy Letters*, 29, 599

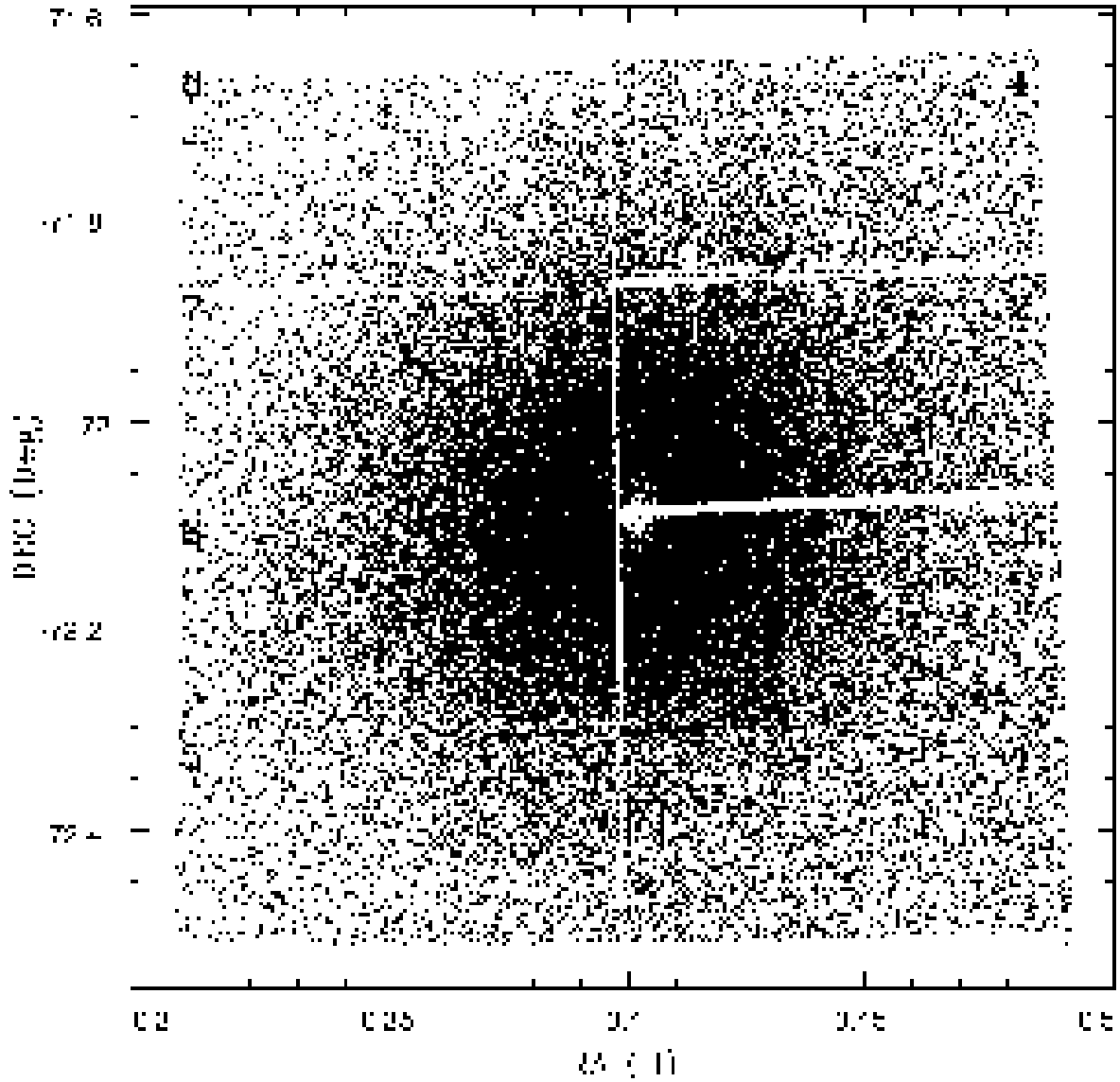


Fig. 1.— Astrometry and layout of the 47 Tuc WFI field; detected variable stars are plotted as triangles. The eight CCDs are labelled numerically. The two regions used to produce the RMS error plot of Fig.3 are indicated as boxes in CCD3 and CCD4. The HST field (Gilliland et al 2000) is marked with a bold box, indicating the significant increase in our field of view compared to those observations. The arrow shows the direction to the core of the SMC.

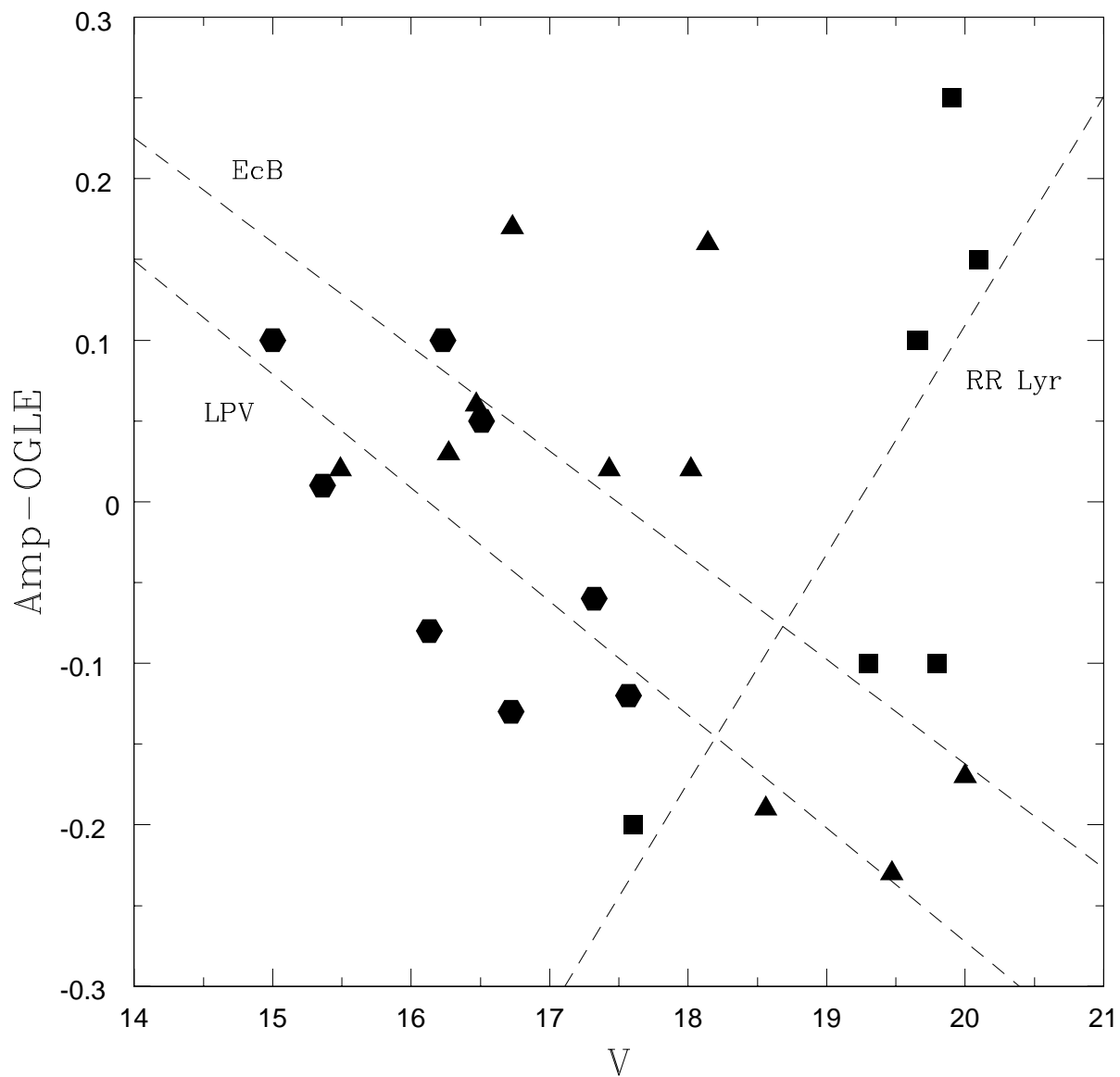


Fig. 2.— A comparison between the total amplitudes of our variables and those cross-identified with Kaluzny et al. (1998). The LPV (hexagons), EcB (triangles) and RR Lyrae (boxes) variables have been plotted and the least-squares fit through the data has been added. If our amplitude is larger than the comparison, the value plotted is  $>0$ . The trends are attributed to the different passbands used (LPV), the presence of different coloured

components (EcB) and to the faintness of the sample (RR Lyraes).

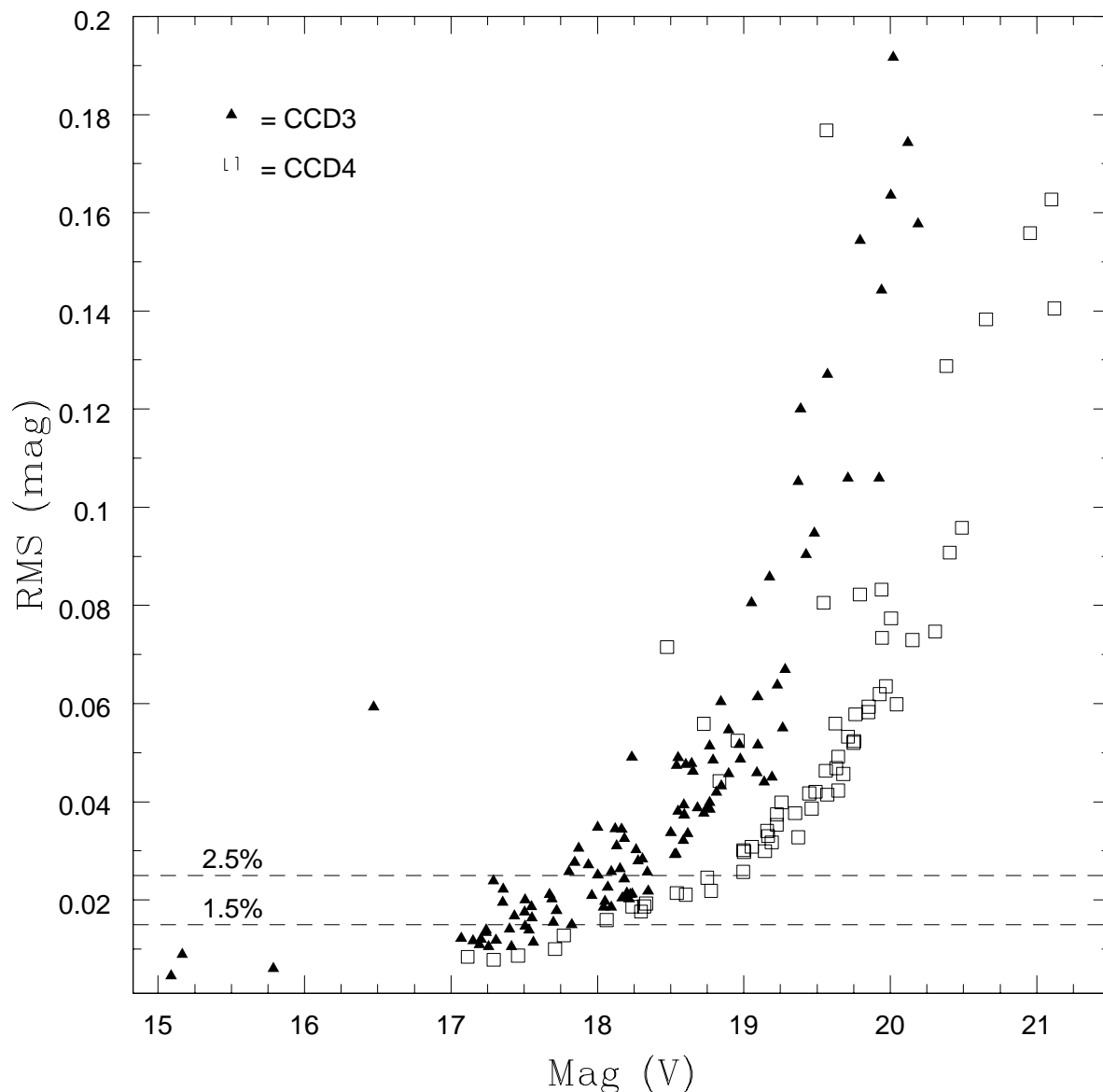


Fig. 3.— Photometric precision, measured as RMS uncertainty for both an inner crowded CCD (triangles) and an outer uncrowded, CCD (squares). At  $V \leq 18.5$ , the quality of the photometry is sufficient in the four inner CCDs to detect a  $\sim 1.5$ - $2.5\%$  dip typical of that caused by an orbiting 'Hot Jupiter' planet or brown dwarf, and is of comparable quality to

$V \leq 19.0$  in the outer four uncrowded CCDs.

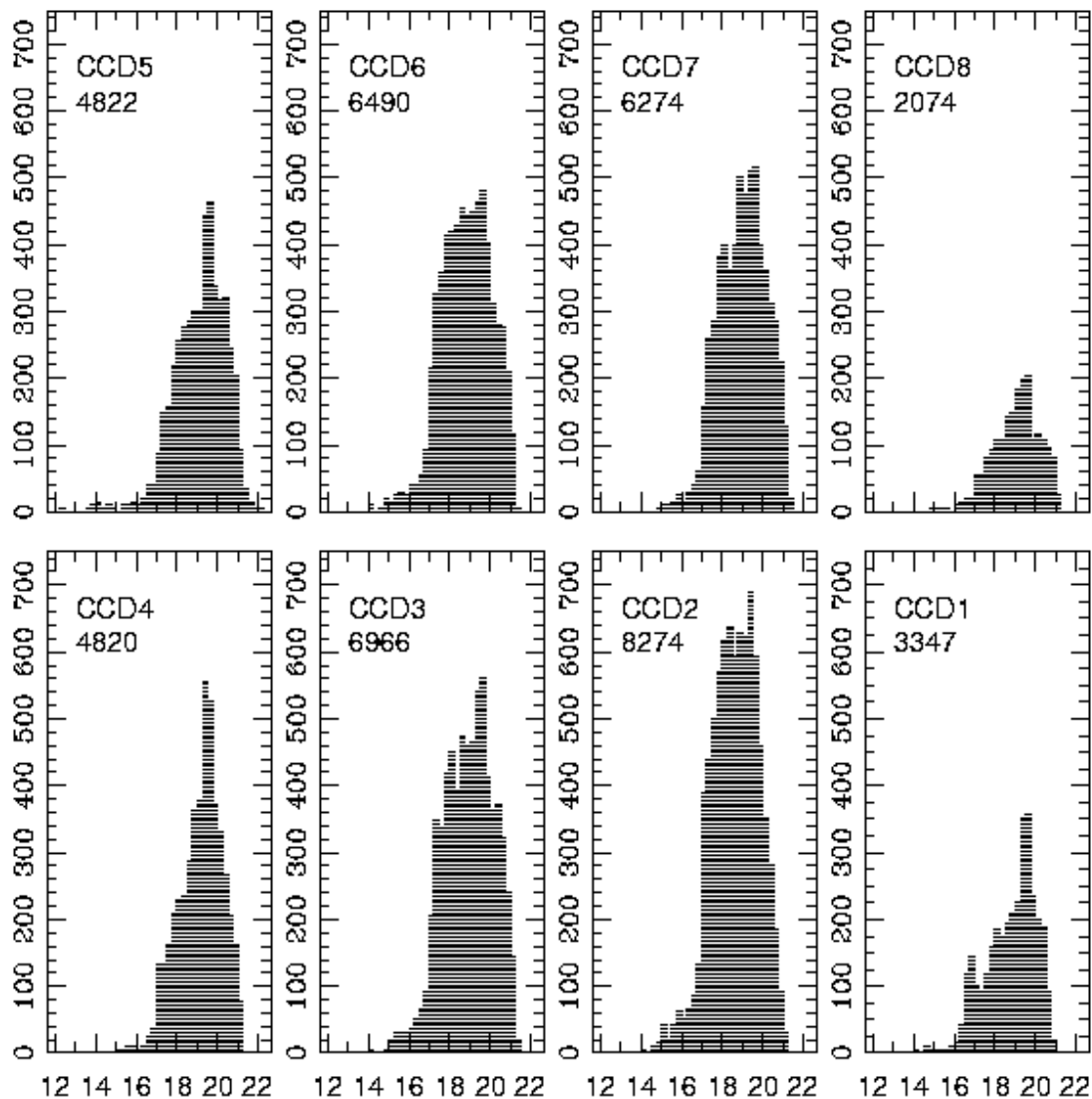


Fig. 4.— As an indication of the depth of our V and I photometric dataset, the number of stars is plotted against magnitude for all eight WFI CCD's, as identified in Fig.1. The dataset is truncated at  $V=21$ , and is saturated at  $V=15$  for CCD4 and  $V=13.5$  for CCD5. The number of stars detected in each CCD is indicated at the top of each subframe.



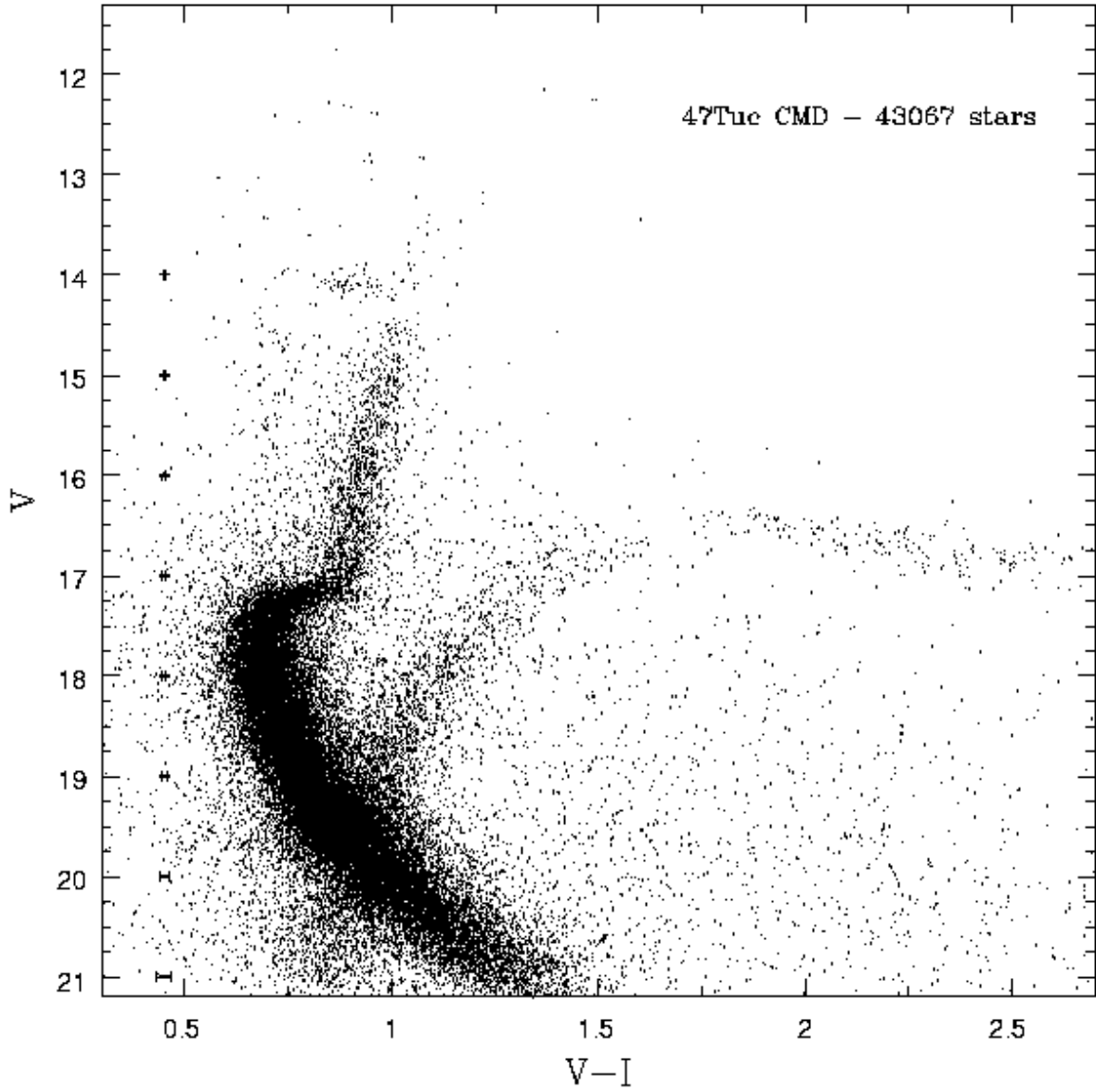


Fig. 5.— Colour Magnitude Diagram dataset used to produce the colour information of the variable stars. The DAOPHOT output RMS errors in our photometry are plotted as errorbars. The calibration is accurate to better than 0.03 mag.

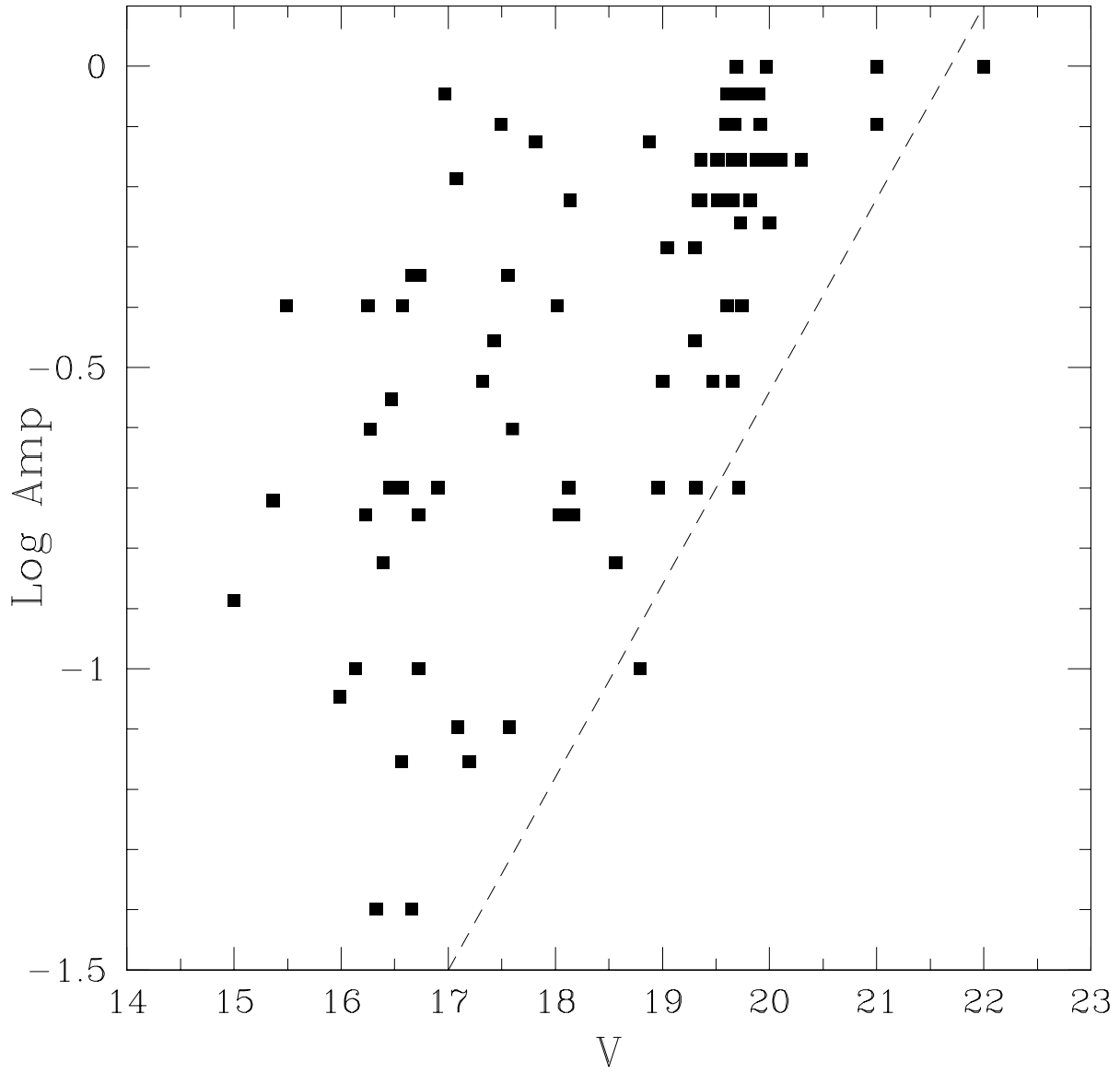


Fig. 6.— The detection limit of our dataset. The dotted line indicates the minimum amplitude a variable must have to be detected as a function of V magnitude in our data. Any amplitudes  $>3\%$  are detectable to a V of 17.0.

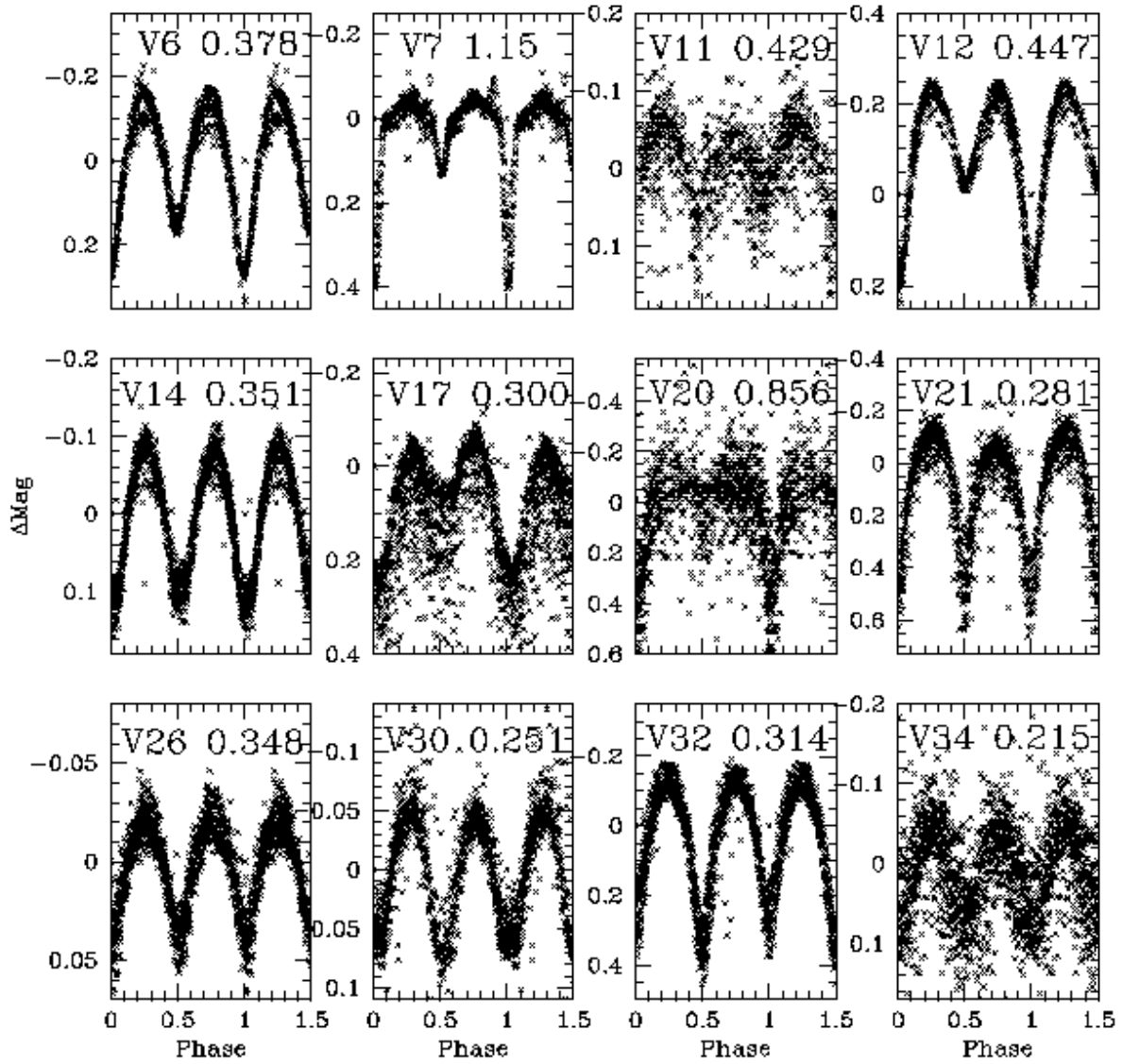


Fig. 7.— Phase wrapped lightcurves of the Eclipsing Binaries detected in our dataset. The identification and period of each star is plotted together with the flux variation in magnitude units.

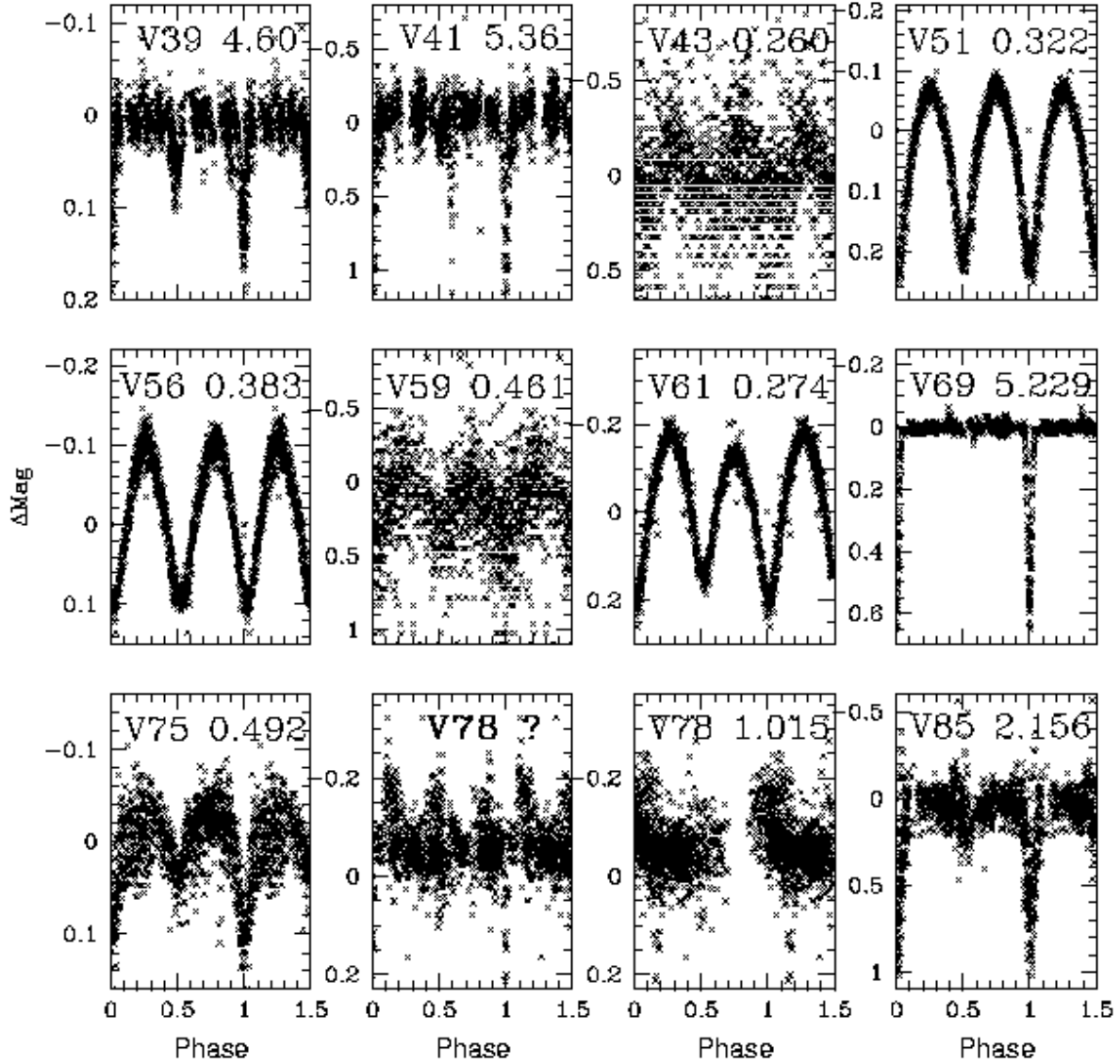


Fig. 8.— Phase-wrapped EcB lightcurves (continued). V78 has an unknown period, as only one eclipse is seen over our sampling range. See Fig.18.

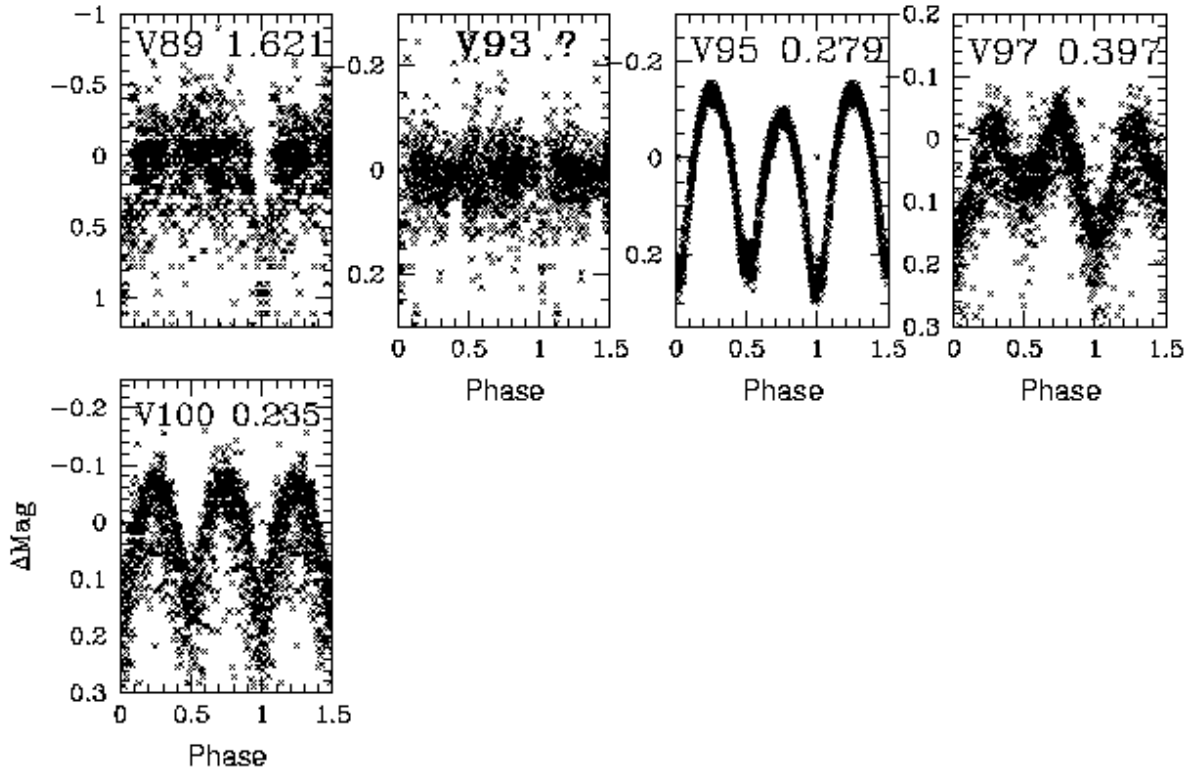


Fig. 9.— Phase-wrapped EcB lightcurves (continued). V93 has an unknown period, as only one eclipse is seen over our sampling range. See Fig.18.

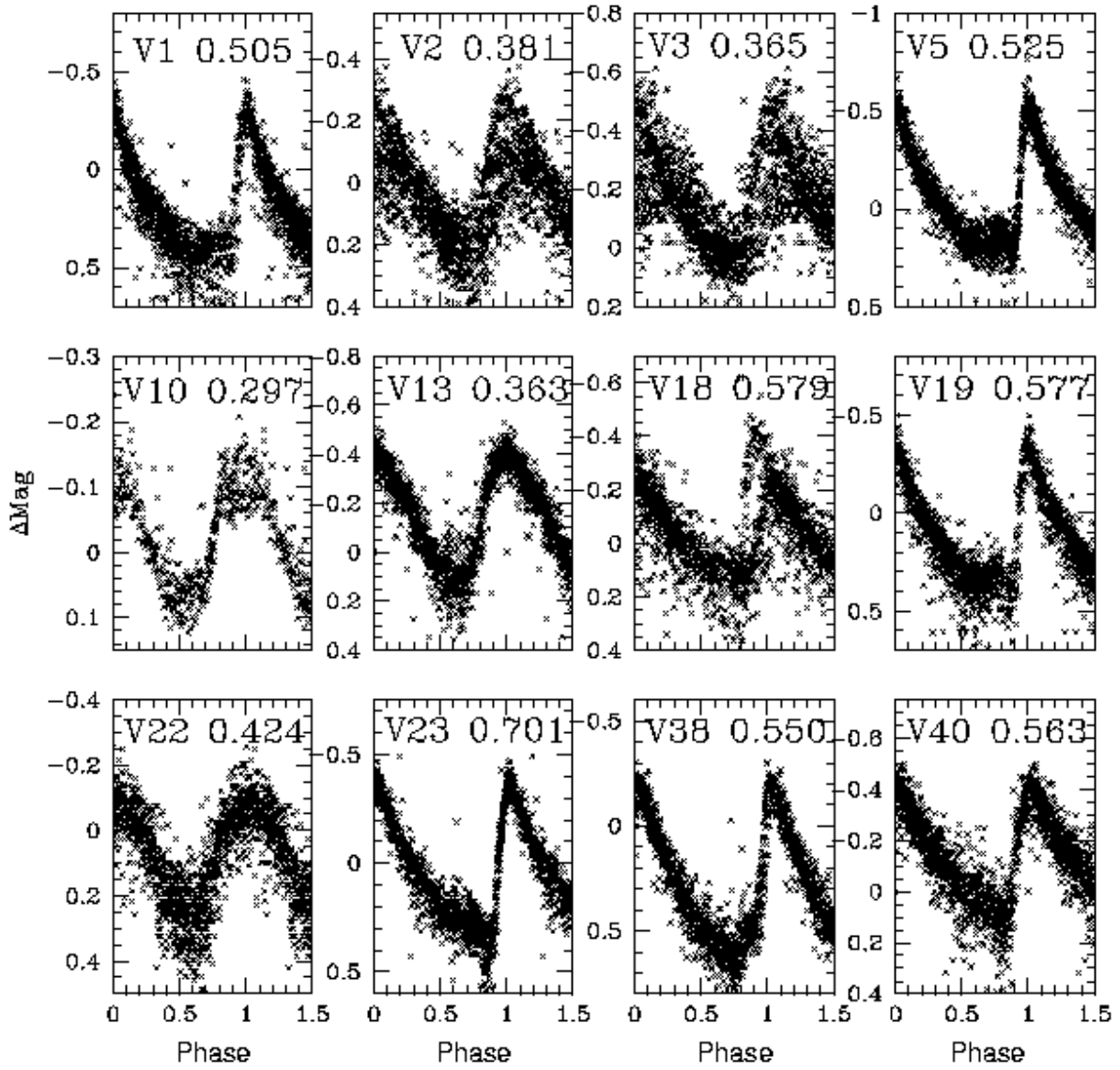


Fig. 10.— Phase-wrapped lightcurves of the RR Lyraes detected in the dataset. The variable identification and the period is indicated.

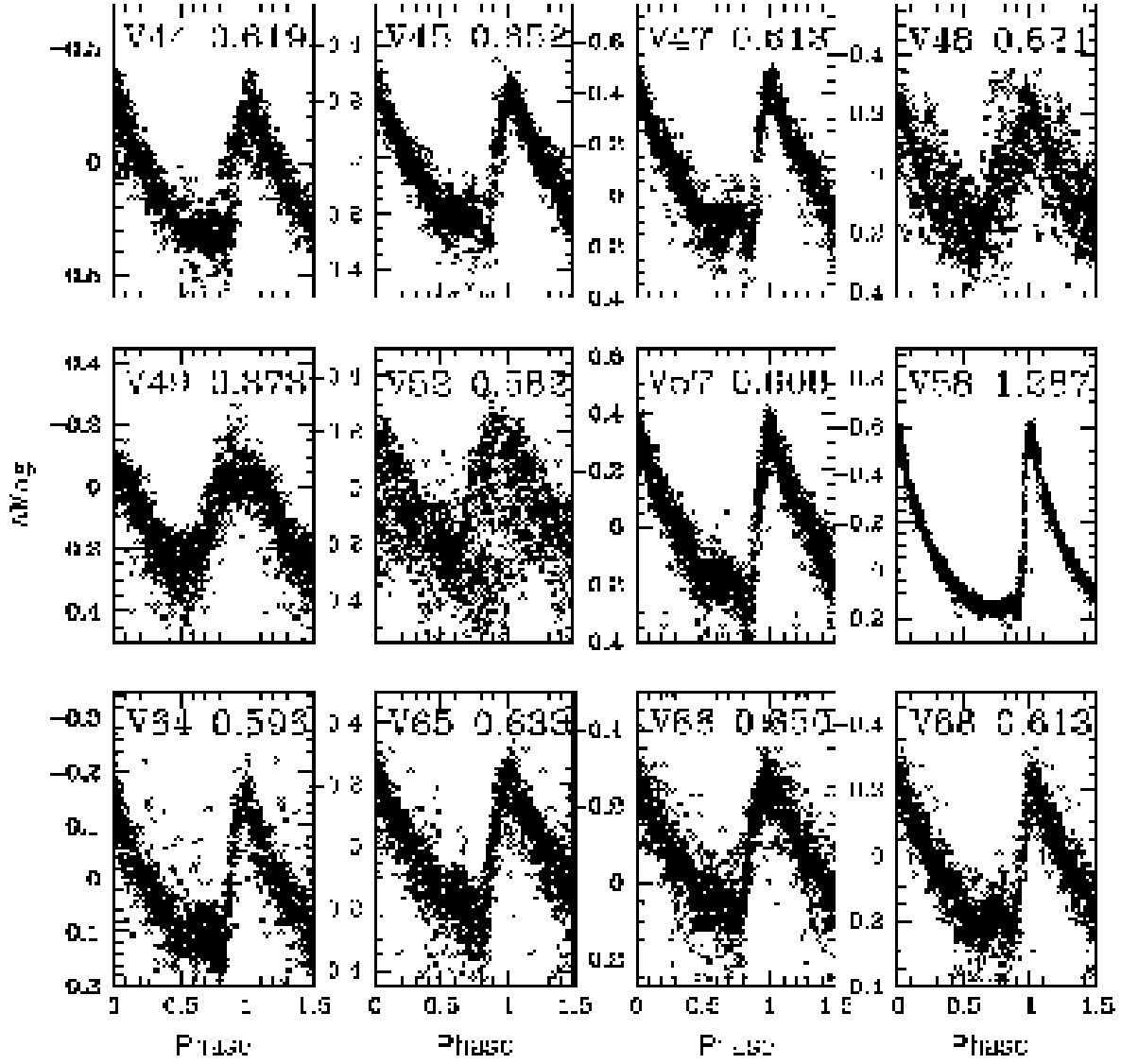


Fig. 11.— Phase-wrapped RR Lyrae lightcurves (continued)

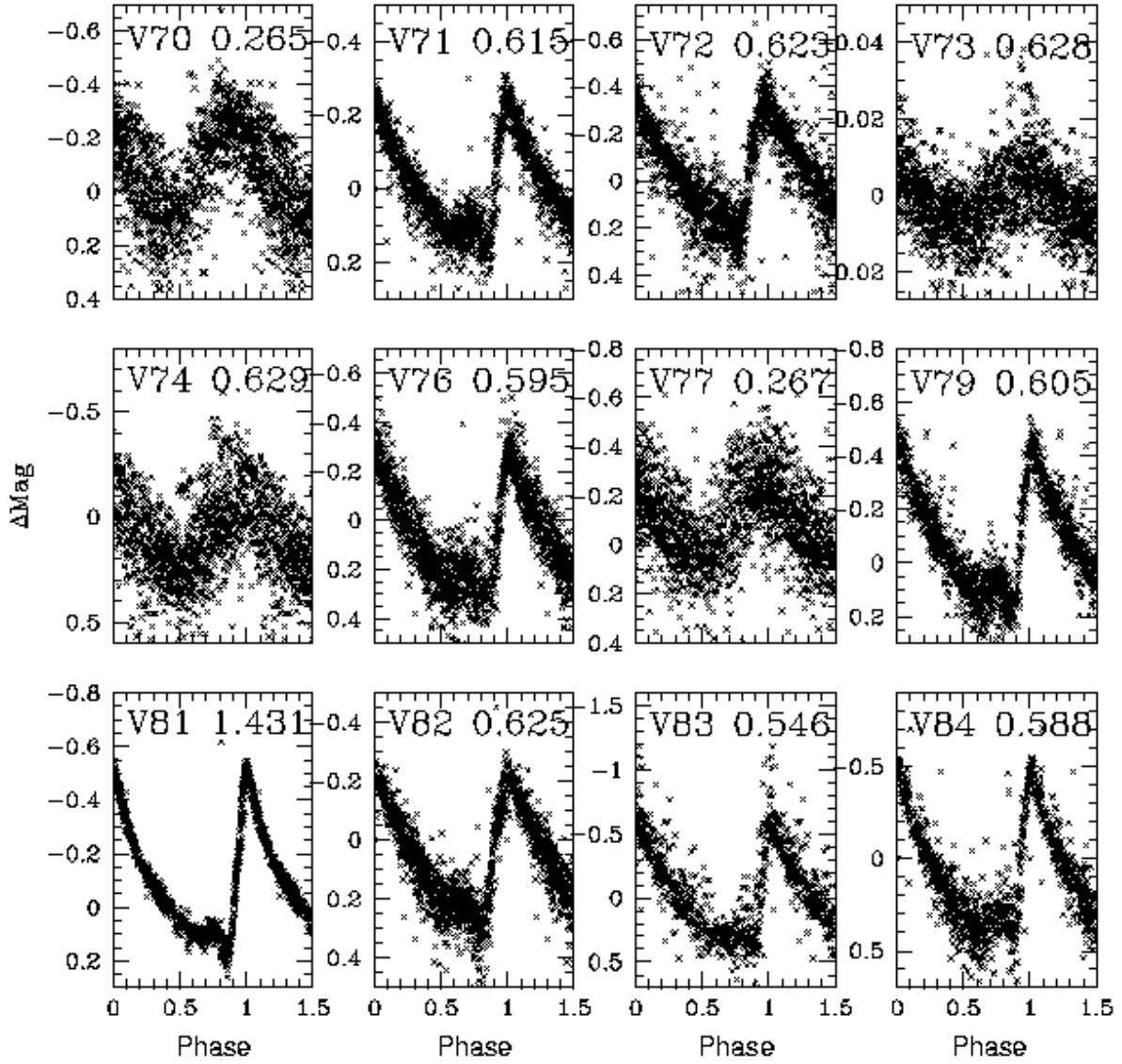


Fig. 12.— Phase-wrapped RR Lyrae lightcurves (continued)



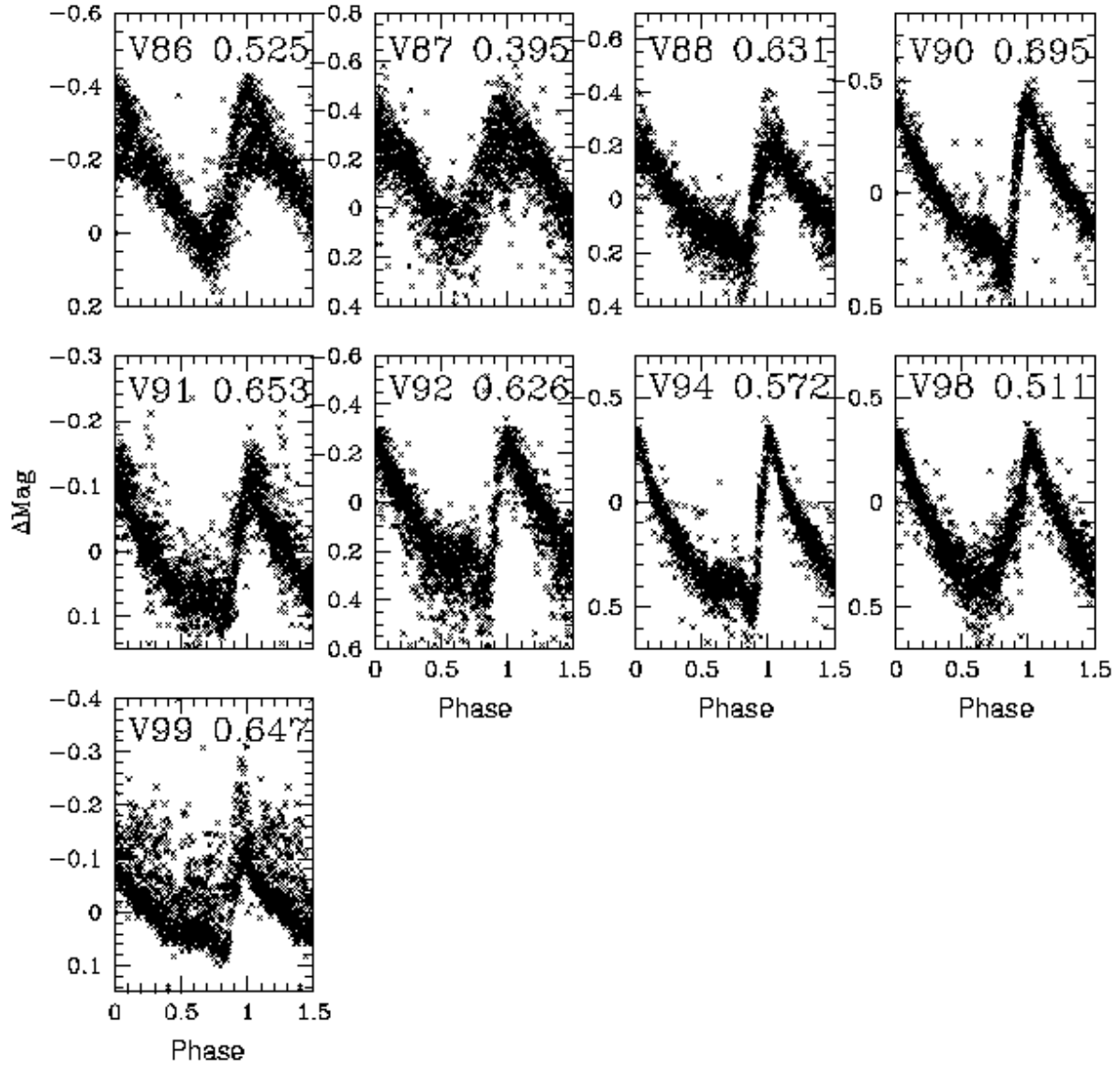


Fig. 13.— Phase-wrapped RR Lyrae lightcurves (continued)

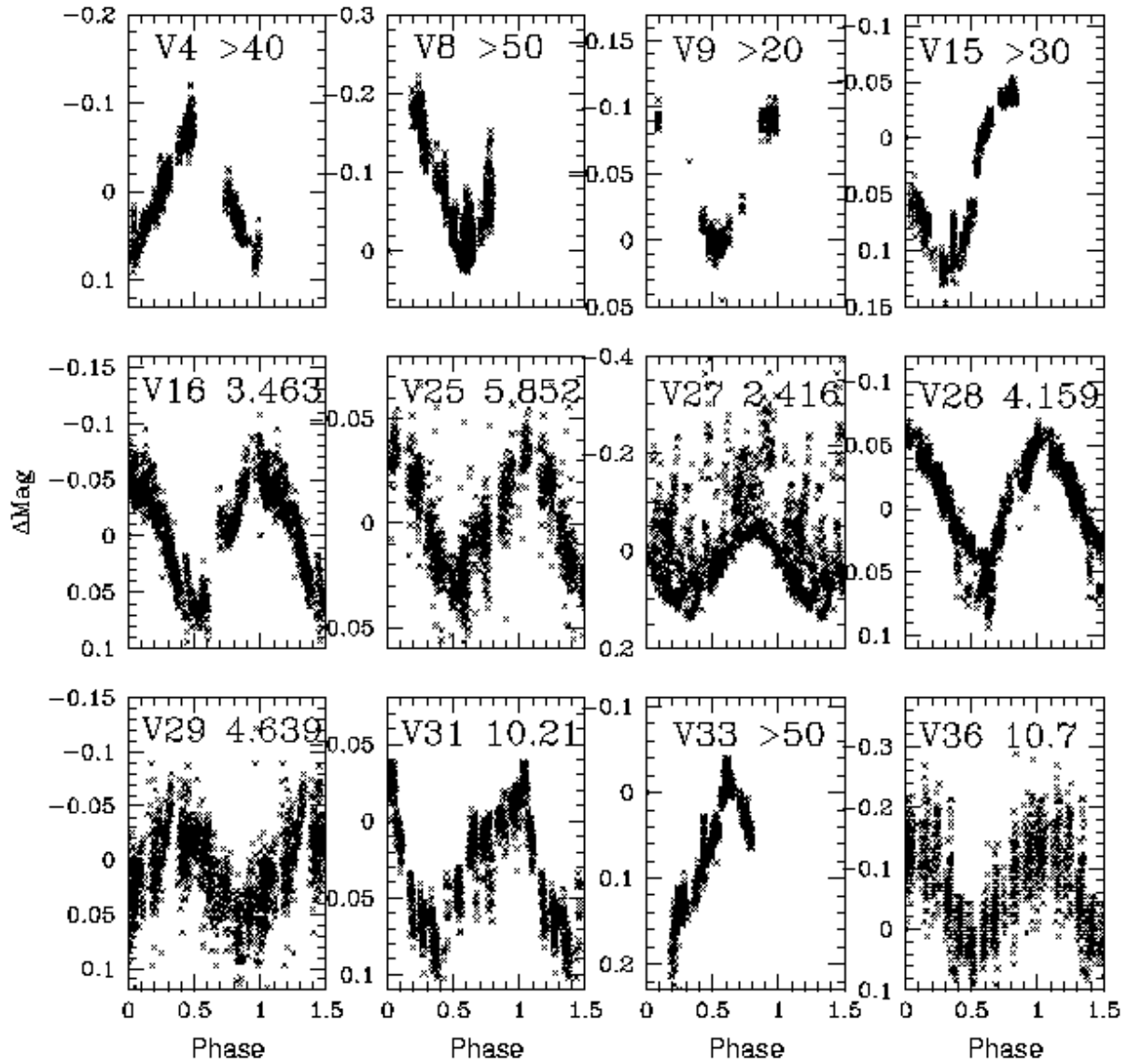


Fig. 14.— Phase-wrapped lightcurves of the Long Period Variables (LPVs) detected in our dataset. The identification and period is indicated.

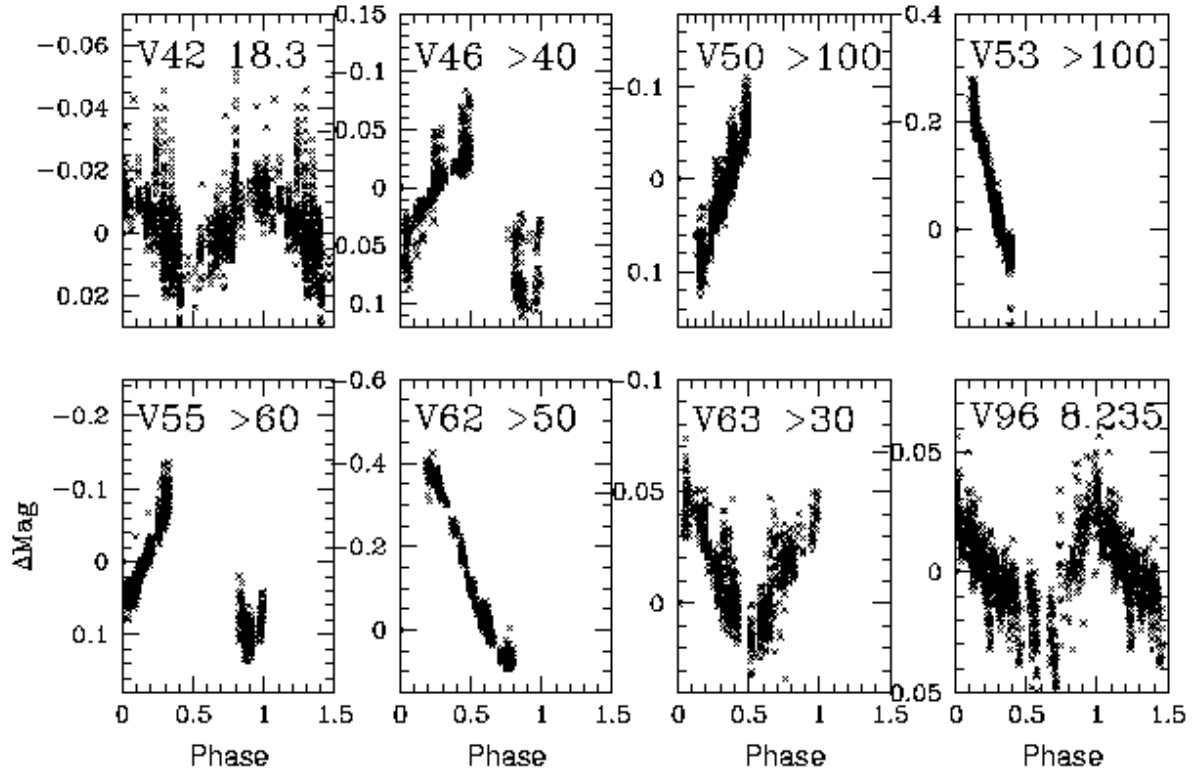


Fig. 15.— Phase-wrapped LPV lightcurve (continued)

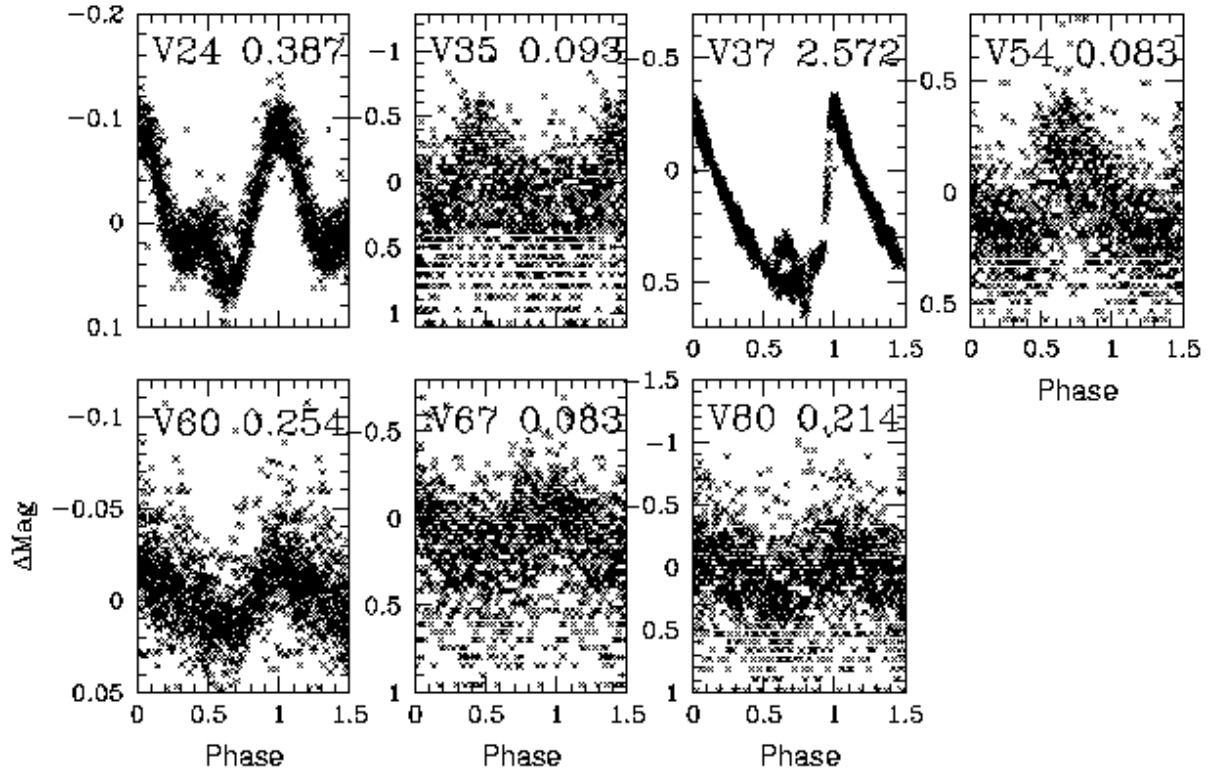


Fig. 16.— Phase-wrapped lightcurves of the miscellaneous variables. The identification and period is indicated.

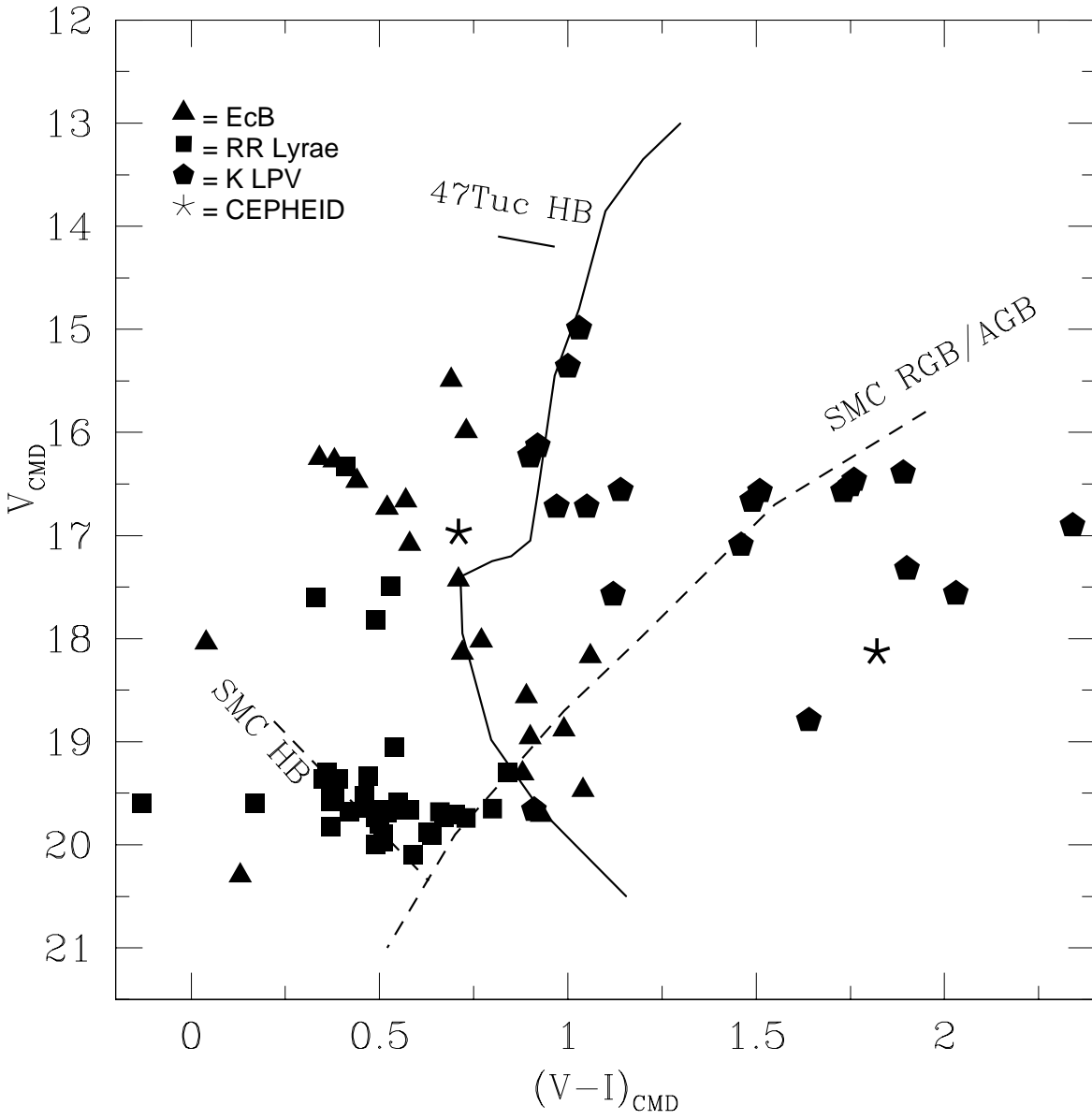


Fig. 17.— Schematic Colour Magnitude Diagram of 47 Tuc, with the location of detected variable stars overplotted. The SMC Red Giant Branch and Horizontal Branch are also marked.

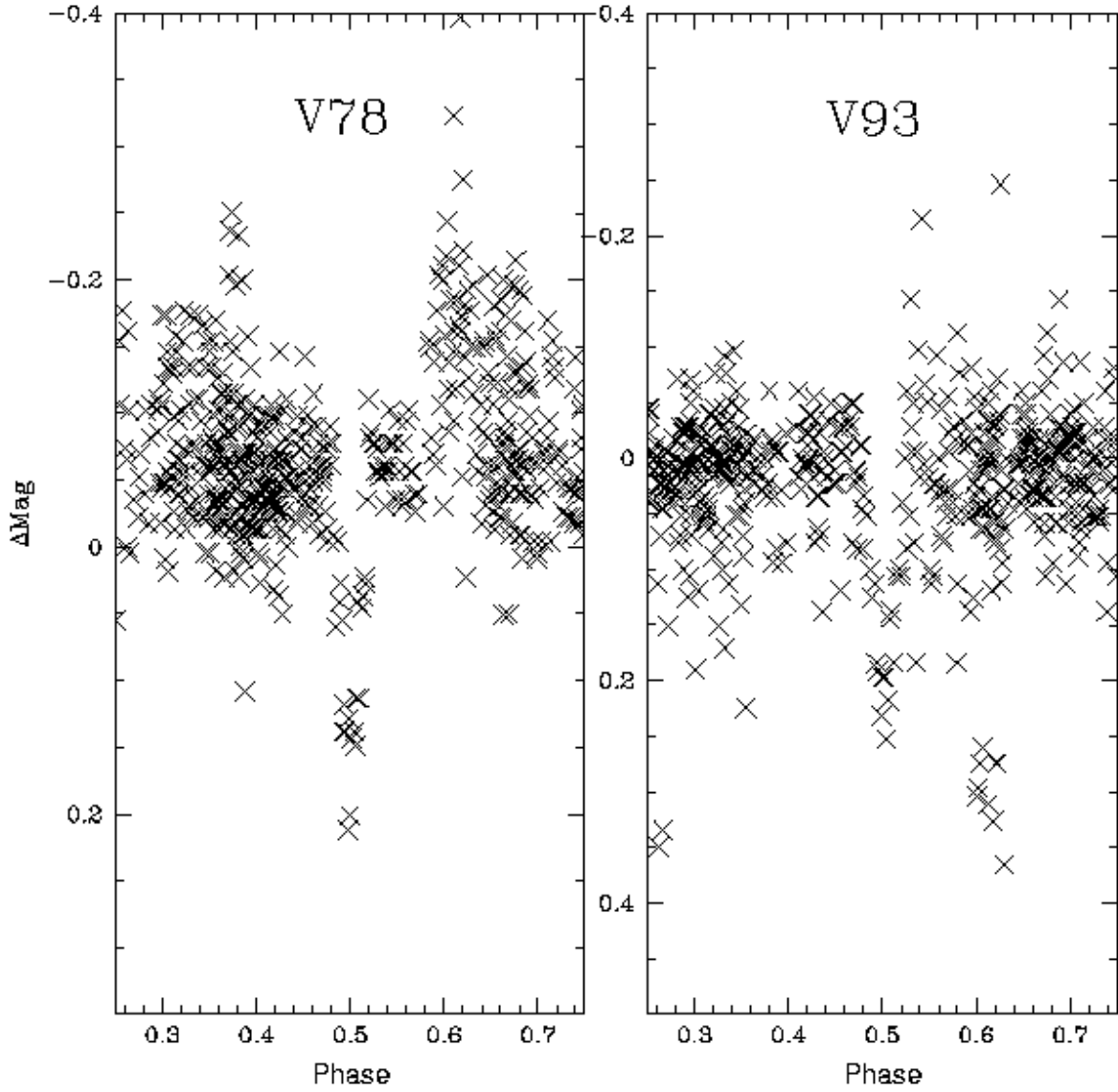


Fig. 18.— V78 and V93, the two variables for which only one eclipse is seen, phase wrapped to the arbitrary values (see text) of 2.794d and 2.419d respectively, plotted to show more detail. The eclipse is likely caused by an M-Dwarf companion.

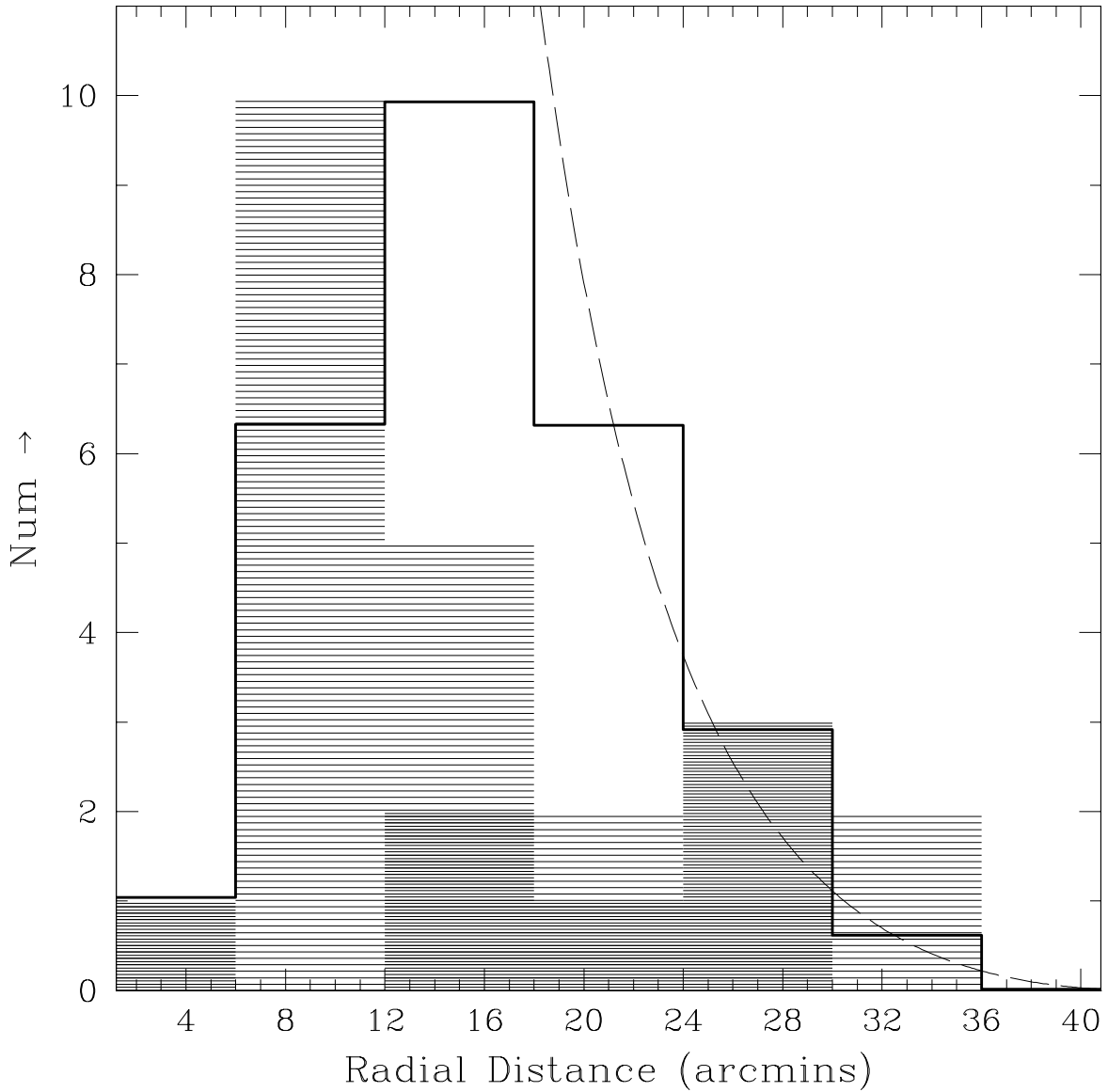


Fig. 19.— Radial distribution of detected EcB stars. The total star distribution (open histogram) is overplotted to the same binning and normalised for comparison, along with a dotted line indicating the theoretical King Profile using parameters determined from Harris (1996). The contact binaries (lighter histogram) are clearly distributed closer to the core than the main stellar population, with the detached EcB systems (dark histogram) being

more segregated to the outer regions of the cluster.

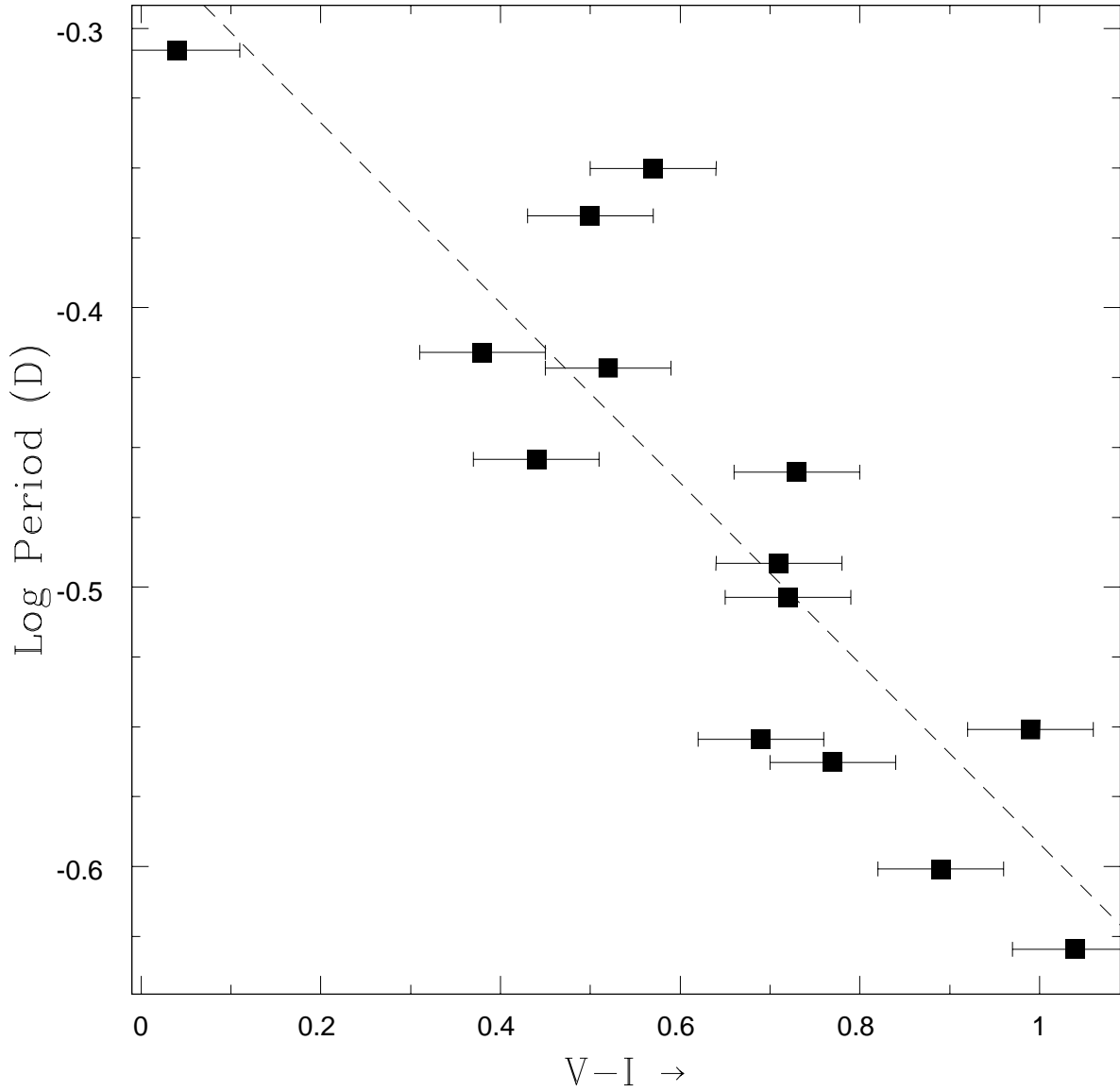


Fig. 20.— Period-Colour diagram of our detected contact binaries. Binary systems are redder the shorter their period. A least-squares fit has been overplotted for completeness.



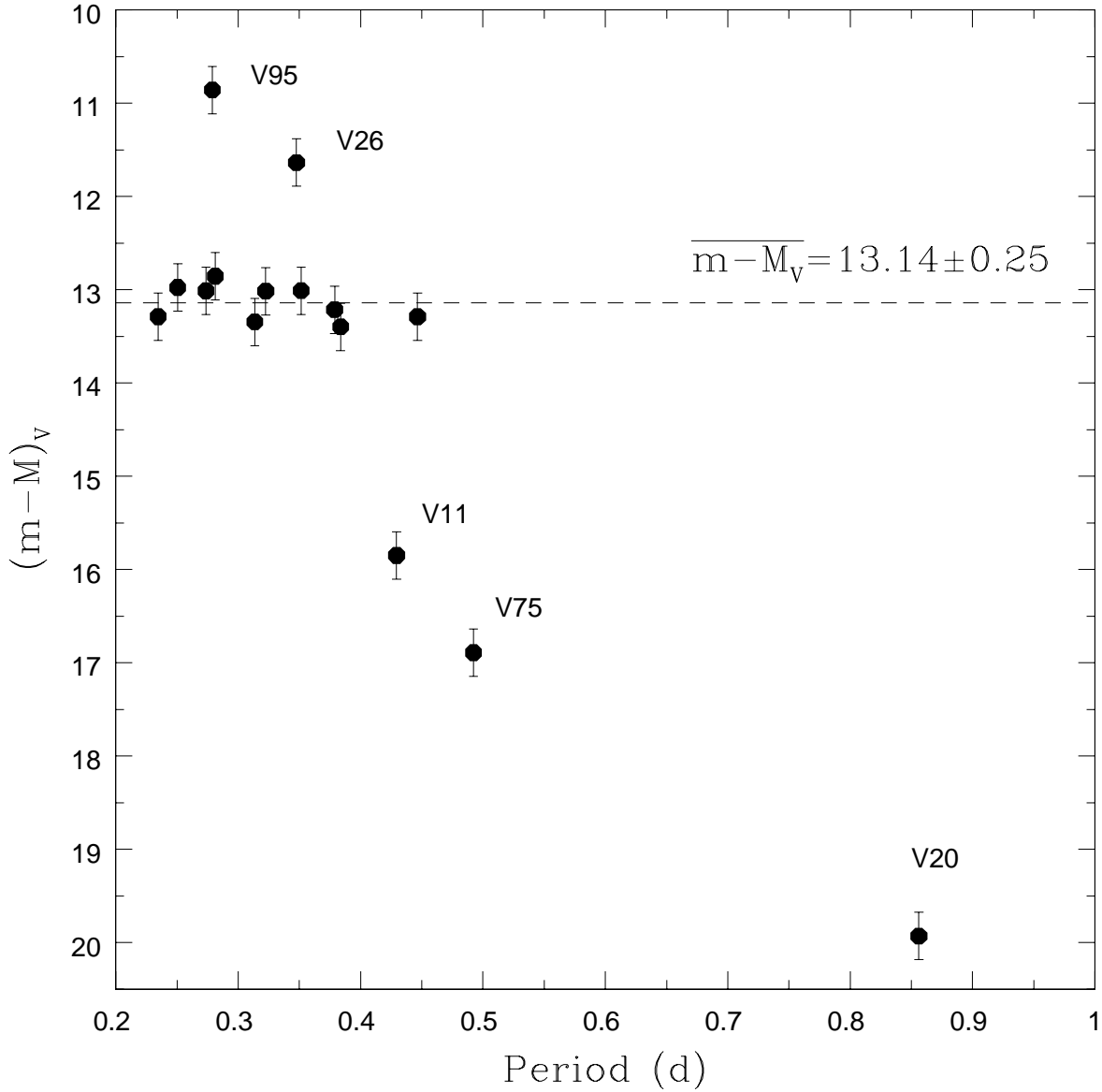


Fig. 21.— The period versus distance modulus diagram for our sample of contact eclipsing binaries. Only those stars with complete colour information and a period  $\leq 1$  day are plotted. The average distance modulus of these 47 Tuc contact binaries is shown as the dashed line. Those systems that are not apparent members of the cluster are identified. V95 and V26 appear to be foreground systems in the Galactic Halo, whereas V11, V75 and V20 are more

likely distant SMC members. The errorbars are the errors associated with the  $M_V$  calculation, and include errors in the colour determination.

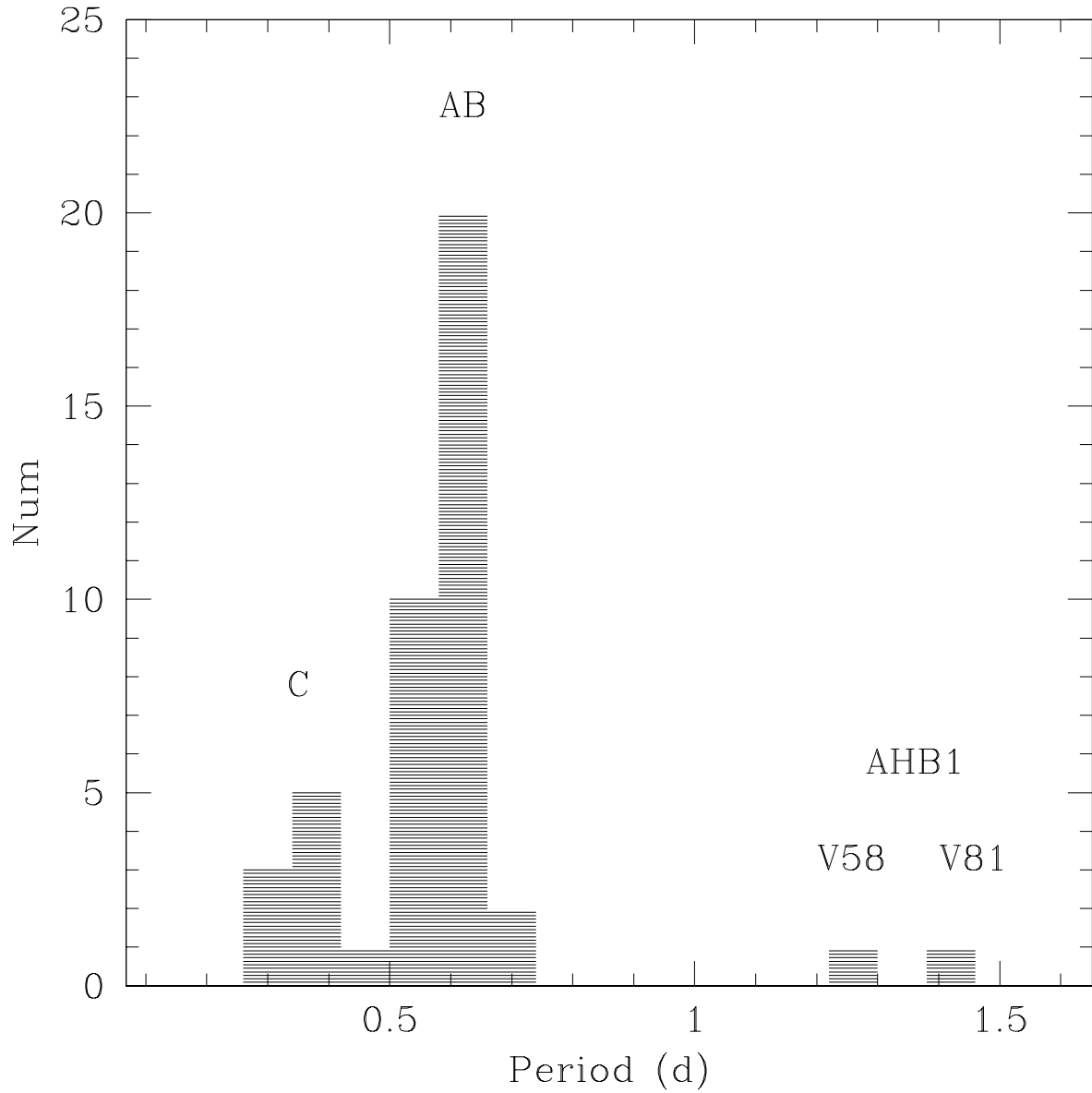


Fig. 22.— Period distribution of detected RR Lyrae stars. Three populations are apparent, and marked accordingly. Two examples of AHB1 stars (both Halo stars) are marked and identified.

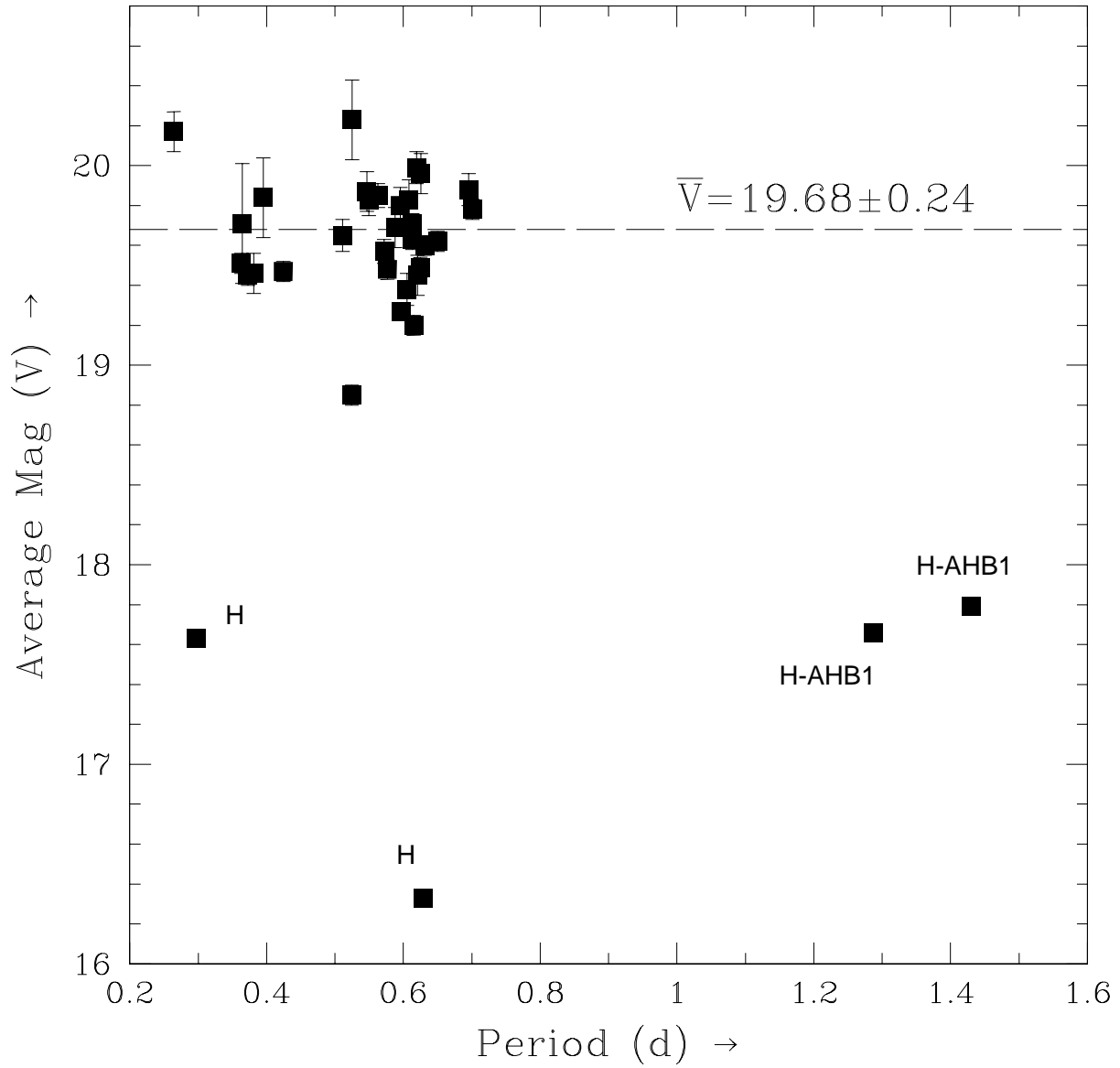


Fig. 23.— Period-Luminosity diagram of those RR Lyrae for which we have magnitude information. The average  $V$  of our SMC RR Lyrae is indicated with a dashed line, along with the identification of Halo stars (H). AHB1 denotes the long-period RR Lyrae described in the text.

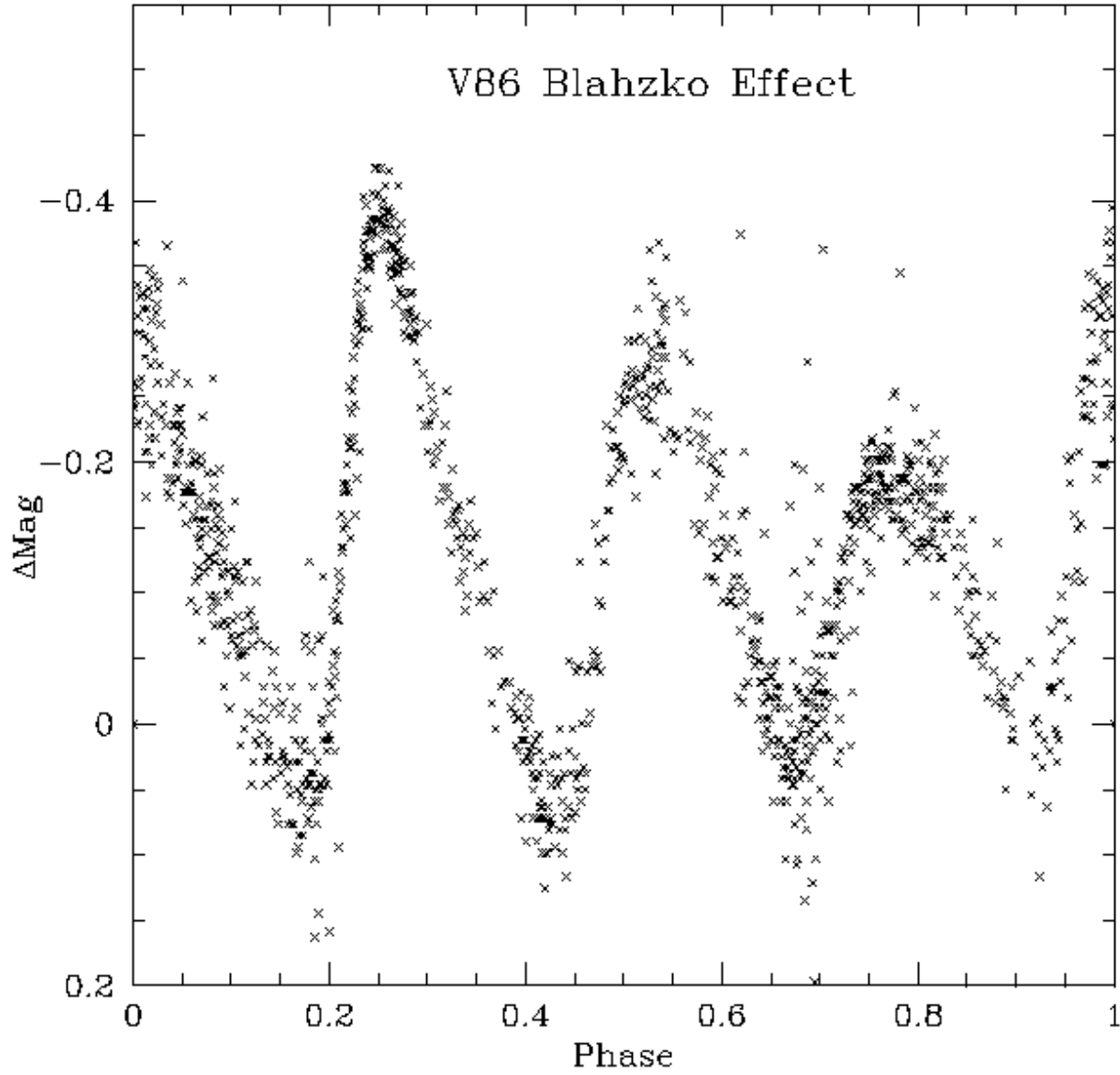


Fig. 24.— Phase-wrapped lightcurve of SMC RR Lyrae V86, showing 4 periods. This star displays a remarkably symmetric Blazhko Effect, every 3 periods the amplitude of variation is significantly lower.

<i>CCD</i>	<i>RA(J2000.0)</i>	<i>DEC(J2000.0)</i>
	h m s	° ' "
1	00:26:40	–71:44:14
2	00:26:40	–71:57:42
3	00:26:40	–72:10:46
4	00:26:40	–72:23:42
5	00:21:02	–72:24:20
6	00:21:02	–72:11:12
7	00:21:02	–71:58:20
8	00:21:02	–71:45:15

Table 1: Equatorial coordinates (J2000.0) for the centres of our CCDs.

<i>ID</i>	<i>Type</i>	<i>RA(J2000.0)</i> h m s	<i>DEC(J2000.0)</i> ° ' "	<i>OGLEGC</i>	<i>CCD</i>
V1	RR Lyr	00:28:52.205	−72:09:31.00	-	3
V2	RR Lyr	00:28:56.555	−72:08:18.75	-	3
V3	RR Lyr	00:28:15.293	−72 06:11.23	-	3
V4	LPV	00:26:19.372	−72:14:02.10	OGLEGC254	3
V5	RR Lyr	00:26:09.379	−72:12:28.64	OGLEGC255	3
V6	EcB	00:26:10.514	−72:11:07.75	OGLEGC227	3
V7	EcB	00:26:08.836	−72:07:01.45	OGLEGC228	3
V8	LPV	00:25:38.176	−72:16:37.62	OGLEGC252	3
V9	LPV	00:25:34.105	−72:09:58.17	OGLEGC222	3
V10	RR Lyr	00:25:42.014	−72:06:01.43	OGLEGC223	3
V11	EcB	00:27:33.659	−72:04:38.26	-	3
V12	EcB	00:26:42.960	−72:15:20.71	OGLEGC253	3
V13	RR Lyr	00:26:56.834	−72:10:13.19	OGLEGC232	3
V14	EcB	00:25:11.146	−72:12:14.42	OGLEGC250	3
V15	LPV	00:25:06.187	−72:10:23.48	OGLEGC219	3
V16	LPV	00:24:31.778	−72:09:29.45	OGLEGC251	3
V17	EcB	00:24:25.499	−72:08:31.60	-	3
V18	RR Lyr	00:29:20.024	−72:00:07.21	-	2
V19	RR Lyr	00:29:02.392	−71:58:57.71	-	2
V20	EcB	00:28:55.205	−71:59:56.93	-	2
V21	EcB	00:29:09.429	−71:51:26.42	-	2
V22	RR Lyr	00:28:31.478	−72:02:07.5	-	2
V23	RR Lyr	00:28:27.374	−71:58:32.19	-	2
V24	TyII Ceph	00:28:15.314	−71:58:21.58	-	2
V25	LPV	00:27:56.580	−71:57:26.71	-	2
V26	EcB	00:26:59.860	−71:55:09.77	-	2
V27	LPV	00:26:12.380	−72:02:13.24	OGLEGC230	2
V28	LPV	00:26:02.920	−72:03:02.94	OGLEGC229	2
V29	LPV	00:25:37.513	−71:56:03.71	-	2
V30	EcB	00:25:15.920	−71:56:06.76	OGLEGC238	2
V31	LPV	00:24:42.540	−71:59:23.92	OGLEGC220	2
V32	EcB	00:25:00.451	−72:00:02.83	OGLEGC221	2
V33	LPV	00:24:36.217	−71:57:19.26	-	2

<i>ID</i>	<i>Type</i>	<i>RA(J2000.0)</i> h m s	<i>DEC(J2000.0)</i> ° ' "	<i>OGLEGC</i>	<i>CCD</i>
V35	$\delta$ Scuti	00:29:06.307	–72:28:48.03	-	4
V36	LPV	00:28:55.595	–72:19:50.77	-	4
V37	Cepheid	00:28:24.641	–72:28:37.04	-	4
V38	RR Lyr	00:28:40.161	–72:24:03.96	-	4
V39	Det.EcB	00:28:21.873	–72:21:28.41	-	4
V40	RR Lyr	00:27:56.936	–72:21:56.20	-	4
V41	Det.EcB	00:27:45.610	–72:23:00.27	-	4
V42	LPV	00:27:38.760	–72:21:46.11	-	4
V43	EcB	00:27:58.730	–72:18:47.36	-	4
V44	RR Lyr	00:27:24.760	–72:23:38.47	-	4
V45	RR Lyr	00:26:56.533	–72:22:08.39	-	4
V46	LPV	00:26:55.296	–72:21:31.04	-	4
V47	RR Lyr	00:26:07.430	–72:24:39.51	-	4
V48	RR Lyr	00:24:48.950	–72:26:42.95	-	4
V49	RR Lyr	00:24:45.564	–72:24:33.29	-	4
V50	LPV	00:25:05.083	–72:26:58.64	-	4
V51	EcB	00:24:58.186	–72:22:11.08	OGLEGC249	4
V52	RR Lyr	00:24:31.318	–72:28:13.25	-	4
V53	LPV	00:24:11.112	–72:27:15.40	-	4
V54	$\delta$ Scuti	00:24:01.445	–72:26:57.49	-	4
V55	LPV	00:23:28.058	–72:26:36.56	OGLEGC248	5
V56	EcB	00:23:15.809	–72:18:53.93	OGLEGC244	5
V57	RR Lyr	00:21:48.627	–72:25:21.48	-	5
V58	RR Lyr	00:21:53.866	–72:22:22.83	-	5
V59	EcB	00:19:26.139	–72:28:52.87	-	5
V60	AGB Puls	00:18:21.268	–72:26:24.44	-	5
V61	EcB	00:22:00.581	–72:02:04.03	OGLEGC214	7
V62	LPV	00:22:11.470	–71:59:17.88	-	7
V63	LPV	00:21:11.387	–72:00:57.68	-	7
V64	RR Lyr	00:21:06.552	–71:56:37.49	-	7
V65	RR Lyr	00:20:49.302	–72:03:09.62	OGLEGC213	7
V66	RR Lyr	00:20:17.035	–71:57:26.36	-	7
V67	$\delta$ Scuti	00:19:09.879	–72:04:27.80	-	7

<i>ID</i>	<i>Type</i>	<i>RA</i> (J2000.0) h m s	<i>DEC</i> (J2000.0) ° ' "	<i>OGLEGC</i>	<i>CCD</i>
V68	RR Lyr	00:18:39.969	−72:03:58.19	-	7
V69	Det.EcB	00:22:52.951	−72:03:40.68	-	7
V70	RR Lyr	00:22:32.785	−71:59:30.94	-	7
V71	RR Lyr	00:22:43.840	−71:57:20.66	OGLEGC234	7
V72	RR Lyr	00:23:36.984	−71:45:14.81	-	8
V73	RR Lyr	00:21:30.496	−71:46:31.43	-	8
V74	RR Lyr	00:20:55.545	−71:41:30.92	-	8
V75	EcB	00:29:05.153	−71:43:25.90	-	1
V76	RR Lyr	00:28:50.459	−71:43:27.06	-	1
V77	RR Lyr	00:28:15.717	−71:46:11.79	-	1
V78	Det.EcB	00:28:21.065	−71:43:40.72	-	1
V79	RR Lyr	00:28:21.180	−71:40:31.50	-	1
V80	δ Scuti	00:26:42.279	−71:44:07.98	-	1
V81	RR Lyr	00:26:42.083	−71:40:24.53	-	1
V82	RR Lyr	00:25:58.078	−71:46:57.09	-	1
V83	RR Lyr	00:28:22.977	−71:28:55.44	-	1
V84	RR Lyr	00:25:11.427	−71:43:35.59	-	1
V85	Det.EcB	00:24:43.872	−71:47:38.26	OGLEGC240	1
V86	RR Lyr	00:24:58.198	−71:42:13.35	-	1
V87	RR Lyr	00:28:23.004	−71:28:22.70	-	1
V88	RR Lyr	00:18:49.569	−72:09:38.80	-	6
V89	Det.EcB	00:18:54.254	−72:06:32.35	-	6
V90	RR Lyr	00:20:57.408	−72:12:04.35	-	6
V91	RR Lyr	00:21:51.437	−72:10:49.96	-	6
V92	RR Lyr	00:21:23.958	−72:15:33.79	OGLEGC243	6
V93	Det.EcB	00:21:07.603	−72:08:55.80	-	6
V94	RR Lyr	00:22:33.373	−72:13:49.70	OGLEGC246	6
V95	EcB	00:22:47.469	−72:13:17.20	OGLEGC245	6
V96	LPV	00:22:40.876	−72:09:22.51	OGLEGC216	6
V97	EcB	00:23:06.015	−72:09:30.52	-	6
V98	RR Lyr	00:23:25.283	−72:19:35.85	OGLEGC247	5
V99	RR Lyr	00:25:49.582	−71:58:27.35	OGLEGC226	2
V100	EcB	00:25:32.213	−72:01:51.37	OGLEGC225	2



Table 2: Table of all detected variable stars in the field of 47 Tuc. Equatorial coordinates given in J2000.0. If the star is previously known, the OGLEGC number is given (Kaluzny et al, 1998). Those marked with a dash are therefore new discoveries. The type of the variable is noted for completion; along with the number of the CCD chip on which it was found. Thirteen of the variable stars found in CCD3 were also independently identified by Eduard Westra, and are presented in his masters thesis 'A search for planets and other variables in 47 Tucanae' (Westra.E.A.M 2003).

<i>ID</i>	<i>Location</i>	<i>Period(d)</i>	$V_{CMD}$	$V - I_{CMD}$	<i>TotalAmp(mag<sub>V+R</sub>)</i>
V6	BS	0.3788	16.73	0.52	0.45
V7	BS	1.1506	16.25	0.34	0.4
V11	BMS	0.4294	18.96	0.50	0.2
V12	BS	0.4465	16.66	0.57	0.45
V14	BS	0.3514	16.47	0.44	0.28
V17	-	0.3005	-	-	0.25
V20	SMC.BS?	0.8561	20.30	0.13	0.7
V21	BMS	0.2812	18.88	0.99	0.75
V26	FGRND?	0.3476	15.99	0.73	0.09
V30	BMS	0.2506	18.56	0.89	0.15
V32	BMS	0.3136	18.14	0.72	0.6
V34	-	0.2155	-	-	0.2
V39	BMS	4.6015	18.17	1.06	0.18
V41	-	5.3648	~21	-	1.0
V43	-	0.2602	-	-	~1
V51	MSTO	0.3226	17.43	0.71	0.35
V56	BS	0.3837	16.27	0.38	0.25
V59	-	0.4618	~21	-	~1
V61	BMS	0.2737	18.02	0.77	0.4
V69	MSTO	5.2239	17.08	0.58	0.65
V75	FGRND?	0.4922	18.04	0.04	0.18
V78	BMS	?	19.31	0.88	0.2
V85	-	2.1559	~20	-	0.55
V89	-	1.6215	~21	-	0.8
V93	BMS	?	19.71	0.93	0.2
V95	FGRND?	0.2789	15.49	0.69	0.4
V97	-	0.3973	~19	-	0.3
V100	BMS	0.2347	19.47	1.04	0.3

Table 3: Table of EcB found in our sample. The likely type is noted as given by the location on the CMD, if data are available for that star. BS=Blue Straggler, BMS=Binary Main Sequence, FGRND=foreground, MSTO=Main Sequence Turnoff. The period is given in days, along with the V magnitude, V-I on the CMD data, and the total amplitude of the variation, measured in magnitudes with a combined Cousins V+R filter.

<i>ID</i>	<i>Period(d)</i>	<i>V<sub>CMD</sub></i>	<i>V – I<sub>CMD</sub></i>	<i>TotalAmp(mag<sub>V+R</sub>)</i>
V1	0.5052	-	-	0.8
V2	0.3812	19.36	0.39	0.6
V3	0.3647	19.36	0.35	0.7
V5	0.5251	19.80	0.50	0.9
V10	0.2971	17.60	0.33	0.25
V13	0.3633	19.66	0.49	0.6
V18	0.5794	-	-	0.6
V19	0.5766	19.63	0.53	0.9
V22	0.4244	19.52	0.37	0.6
V23	0.7008	19.68	0.66	0.9
V38	0.5495	19.60	0.17	0.9
V40	0.5627	19.82	0.37	0.6
V44	0.6190	19.91	0.64	0.8
V45	0.6524	-	-	0.6
V47	0.6129	19.88	0.63	0.7
V48	0.6210	19.58	0.37	0.6
V49	0.3727	19.60	-0.13	0.4
V52	0.5820	19.64	0.46	0.6
V57	0.6084	19.66	0.58	0.7
V58	1.2875	17.49	0.53	0.8
V64	0.5963	19.30	0.84	0.35
V65	0.6327	-	-	0.5
V66	0.6503	19.74	0.73	0.4
V68	0.6131	19.73	0.67	0.55
V70	0.2653	-	-	0.6
V71	0.6151	19.30	0.36	0.5
V72	0.6227	-	-	0.55
V73	0.6283	16.33	0.41	0.04
V74	0.6291	19.73	0.49	0.7
V76	0.5954	19.68	0.42	0.8
V77	0.2645	20.00	0.49	0.7
V79	0.6053	19.59	0.55	0.8
V81	1.4301	17.82	0.49	0.75
V82	0.6252	19.33	0.47	0.6

<i>ID</i>	<i>Period(d)</i>	<i>V<sub>CMD</sub></i>	<i>V – I<sub>CMD</sub></i>	<i>TotalAmp(mag<sub>V+R</sub>)</i>
V83	0.5465	19.97	0.51	1.0
V84	0.5882	19.69	0.52	1.0
V86	0.5247	19.05	0.54	0.5
V87	0.3951	19.51	0.38	0.7
V88	0.6313	19.52	0.46	0.7
V90	0.6952	19.70	0.70	0.9
V91	0.6533	-	-	0.3
V92	0.6256	20.10	0.59	0.7
V94	0.5721	19.65	0.80	0.9
V98	0.5114	19.90	0.51	0.9
V99	0.6475	-	-	0.25

Table 4: Table of RR Lyraes found in our data. The ID, period, colour, V magnitude as per the CMD dataset, if known, and total variability amplitude are noted.

<i>ID</i>	<i>Period(d)</i>	<i>V<sub>CMD</sub></i>	<i>V – ICMD</i>	<i>TotalAmp(mag<sub>V+R</sub>)</i>
V4	>40	16.51	1.75	0.2
V8	>50	17.32	1.90	>0.3
V9	>20	16.13	0.92	>0.1
V15	>30	15.36	1.00	0.19
V16	3.4629	16.72	1.05	0.18
V24	0.3871	18.13	1.82	0.2
V25	5.8524	16.72	0.97	0.1
V27	2.416	17.57	1.12	0.08
V28	4.159	15.00	1.03	0.13
V29	4.639	18.79	1.64	0.1
V31	10.21	16.23	0.90	0.18
V33	>50	16.57	1.51	>0.2
V35	0.0932	~22	-	1.0
V36	10.7	19.66	0.91	0.3
V37	2.5724	16.97	0.71	0.9
V42	18.3	16.66	1.49	0.04
V46	>40	16.39	1.89	>0.15
V50	>100	16.90	2.34	>0.2
V53	>100	16.57	1.73	>0.4
V54	0.0834	~21	-	1.0
V55	>60	16.46	1.76	>0.2
V60	0.2544	17.20	2.99	0.07
V62	>50	17.56	2.03	>0.45
V63	>30	17.09	1.46	>0.08
V67	0.0829	~20	-	0.7
V80	0.2144	~22	-	~1
V96	8.235	16.56	1.14	0.07

Table 5: Table of LPV’s and the other miscellaneous variables. The ID, period, colour, V

magnitude as per the CMD dataset, if known, and total variability amplitude are noted.